REPORT DOCUMENTATION PAGE

Form Approved
OMB No. 0704-0188

1. REPORT DATE *(DD-MM-YYYY)*	**2. REPORT TYPE**	**3. DATES COVERED** *(From - To)*
29-06-2015	master's thesis	May 2009 - December 2011

4. TITLE AND SUBTITLE

Frequency Diverse Array Receiver Architectures

5a. CONTRACT NUMBER

5b. GRANT NUMBER

5c. PROGRAM ELEMENT NUMBER

6. AUTHOR(S)

Aaron M. Jones, DR-II
Research Physicist
aaron.jones.41@us.af.mil
937-528-8571

5d. PROJECT NUMBER

5e. TASK NUMBER

5f. WORK UNIT NUMBER

7. PERFORMING ORGANIZATION NAME(S) AND ADDRESS(ES)

Air Force Research Laboratory
Sensors Directorate (AFRL/RYAP), Mr. Aaron Jones
Wright-Patterson AFB, OH, 45433
937-528-8571 and aaron.jones.41@us.af.mil

8. PERFORMING ORGANIZATION REPORT NUMBER

9. SPONSORING / MONITORING AGENCY NAME(S) AND ADDRESS(ES)

Air Force Research Laboratory
Sensors Directorate (AFRL/RYAP), Dr. Jeffrey Sanders
Wright-Patterson AFB, OH, 45433
937-528-8571 and jeffrey.sanders.12@us.af.mil

10. SPONSOR/MONITOR'S ACRONYM(S)

AFRL / RYAP

11. SPONSOR/MONITOR'S REPORT NUMBER(S)

12. DISTRIBUTION / AVAILABILITY STATEMENT

APPROVED FOR PUBLIC RELEASE; DISTRIBUTION UNLIMITED

13. SUPPLEMENTARY NOTES

14. ABSTRACT

Typical radar systems are limited to energy distribution characteristics that are range independent. However, operators are generally interested in obtaining information at particular ranges and discarding elsewhere. It seems appropriate then to attempt to put energy solely at the range(s) of interest, thus minimizing exposure to clutter, jammers and other range-dependent interferences sources. The frequency diverse array (FDA) can provide a mechanism to achieve range-dependent beamforming and the spatial energy distribution properties are investigated on transmit and receive for different architectures herein. While simplified FDA receive architectures have been explored, they exclude the return signals from transmitters that are not frequency matched. This practice neglects practical consideration in receiver implementation and has motivated research to formulate a design that includes all frequencies. We present several receiver architectures for a uniform linear FDA, and compare the processing chain and spatial patterns in order to formulate an argument for the most efficient design to maximize gain on target.

15. SUBJECT TERMS

RADAR, FREQUENCY DIVERSE ARRAY, WAVEFORM DIVERSITY, ANTENNA PATTERNS

16. SECURITY CLASSIFICATION OF:			**17. LIMITATION OF ABSTRACT**	**18. NUMBER OF PAGES**	**19a. NAME OF RESPONSIBLE PERSON**
a. REPORT	**b. ABSTRACT**	**c. THIS PAGE**			Mr. Aaron M. Jones, Research Physi
U	U	U	UU	72	**19b. TELEPHONE NUMBER** *(include area code)* 937-528-8571

Frequency Diverse Array Receiver Architectures

A thesis submitted in partial fulfillment
of the requirements for the degree of
Master of Science in Engineering

by

AaronM. Jones
Department of Electrical Engineering and Computer Science
B.S. Engineering Physics, Wright State University, 2007

2011
Wright State University

Wright State University
SCHOOL OF GRADUATE STUDIES

November 18, 2011

I HEREBY RECOMMEND THAT THE THESIS PREPARED UNDER MY SUPERVISION BY AaronM. Jones ENTITLED Frequency Diverse Array Receiver Architectures BE ACCEPTED IN PARTIAL FULFILLMENT OF THE REQUIREMENTS FOR THE DEGREE OF Master of Science in Engineering.

Brian D. Rigling, Ph.D.
Thesis Director

Kefu Xue, Ph.D.
Department Chair of Electrical Engineering

Committee on
Final Examination

Brian D. Rigling, Ph.D.

Fred Garber, Ph.D.

Douglas T. Petkie, Ph.D.

Andrew Hsu, Ph.D.
Dean, Graduate School

ABSTRACT

Jones, Aaron M., M.S.Egr, Department of Electrical Engineering and Computer Science, Wright State University, 2011. *Frequency Diverse Array Receiver Architectures.*

Typical radar systems are limited to energy distribution characteristics that are range independent. However, operators are generally interested in obtaining information at particular ranges and discarding elsewhere. It seems appropriate then to attempt to put energy solely at the range(s) of interest, thus minimizing exposure to clutter, jammers and other range-dependent interferences sources. The frequency diverse array (FDA) can provide a mechanism to achieve range-dependent beamforming and the spatial energy distribution properties are investigated on transmit and receive for different architectures herein.

While simplified FDA receive architectures have been explored, they exclude the return signals from transmitters that are not frequency matched. This practice neglects practical consideration in receiver implementation and has motivated research to formulate a design that includes all frequencies. We present several receiver architectures for a uniform linear FDA, and compare the processing chain and spatial patterns in order to formulate an argument for the most efficient design to maximize gain on target.

It may also be desirable to beamsteer in higher dimensionalities than a linear array affords, thus, the transmit and receive concept is extended to a generic planar array. This new architecture allows 3-D beamsteering in angle and range while maintaining practicality. The spatial patterns that arise are extremely unique and afford the radar designer an additional degree of freedom to develop operational strategy.

The ability to simultaneously acquire, track, image and protect assets is a requirement of future fielded systems. The FDA architecture intrinsically covers multiple diversity domains therefore, naturally lends it self to a multi-mission, multi-mode radar scheme. A multiple beam technique that uses coding is suggested to advance this notion.

List of Symbols

Chapter 1

FDA	frequency diverse array
$STAP$	space-time, adaptive processing
LFM	linear frequency modulation

Chapter 2

SAR	synthetic aperture radar
$GMTI$	ground, moving-target indicator
ULA	uniform linear array
$\phi^{'}$	apparent scan angle
R	range
c	speed of light
Δf	linear frequency step
LPI	low probability of intercept
$MIMO$	multiple-input, multiple-output
$HMPAR$	hybrid MIMO phased array radar

Chapter 3

CW	continuous wave
t	time
d	inter-element spacing
λ_{min}	minimum wavelength
f_n	set of transmit frequencies from a linear array
f_c	carrier frequency
N	number of elements in the array
s_n	transmit signal from each element
R_n	range from each element to a target location
θ_o	angle off boresight of target
α	transmit beam-weighting factor
s	composite transmit signal
λ_c	wavelength of carrier frequency
ω_f	$\pi\Delta f$
ω_o	$\frac{\pi d}{\lambda_c}$
CF	constant frequency
FD	frequency diverse
SNR	signal-to-noise ratio
r_m	received signal at each element
M	number of receive elements
h_m^*	filter for receive architecture *
v_m^*	filtered received signal at each element for architecture *
β_m^*	receive beam-weighting at each element for architecture *
y^*	composite received signal for architecture *
H_m	filter bank for each receive element

Chapter 4

d_y	Y-axis inter-element spacing
d_x	X-axis inter-element spacing
f_{nm}	transmit frequency for the nm element
Δf_x	frequency offset along X-axis
Δf_y	frequency offset along Y-axis
N	number of elements along X-axis
M	number of elements along Y-axis
P	receive element along X-axis
Q	receive element along Y-axis
y_{pq}	receive signal at each element

Chapter 5

f_{ln}	set of transmit frequencies for each beam and element
F_l	carrier frequency for each beam
Δf_l	offset frequency for each beam
L	number of beams
c_l	orthogonal code sequence for each beam
f_s	code sampling rate
T	length of code
C	integration amplitude scaling factor

Contents

List of Figures

List of Tables

Acknowledgement

It is my pleasure to thank those who helped effectuate this research project, without whom it would not have been possible. First, I would like to thank the team of individuals who solicited me to this project, primarily, Mr. William J. Baldygo and Mr. Jonathan E. Scanlan. It was their motivation that inspired me to continue my education, pursue this topic and ultimately develop the receive architectures contained herein.

I am also indebted to many of my current and former colleagues especially the Branch Chief, Dr. Jeffrey H Sanders and Technical Advisor, Dr. Muralidhar Rangaswamy of the RF Exploitation Technology Branch within AFRL who supported the advancement of this technology and afforded me the time to complete this thesis.

Additionally, I would like to thank Mr. Keith D. Sawmiller, Mr. Michael J. Callahan and Mr. Jason T. Parker who all have contributed, in their own way, to my professional and sometimes personal development.

I owe sincere gratitude to my advisor, Dr. Brian D. Rigling, who has committed countless hours both in the classroom and in personal correspondence to my technical development. Dr. Rigling is a true teacher, evident by his patience, knowledge and selflessness to help others grow and achieve, he provided the gusto needed to complete this program of study. I also thank Dr. Douglas T. Petkie and Dr. Fred Garber for their participation on the thesis committee.

Lastly, I would like to thank my family, especially my beautiful wife, Lesley. Without her support, confidence, love and ability to fill our home with warmth, I would not have been able realize this achievement.

Dedicated to

Lesley and Cameron and Michael

Chapter 1

Introduction

The radar problem implies the need to operate in complex environments with uncooperative targets of interests in order to locate, track and glean additional information about the scene utilizing only radio frequencies and the algorithms at your disposal. As this problem becomes more difficult, either by the requirements placed on the system or the limits of the operating space, the ability to efficiently use the information and energy available to the radar designer becomes a higher priority.

The frequency diverse array (FDA) provides an additional degree of freedom to efficiently gather and therefore potentially use, scene information. But, here-to-date, the research has limited the receive architecture to designs that prohibit all signals and information from being available for processing. This severely undermines potential FDA capability and motivates research to consider additional architectures.

Furthermore, as operating environments become increasingly complex, the ability to control range-angle dependent energy distribution becomes an increasingly desirable trait. While techniques exist to assist in mitigating range-dependent effects, such as STAP, they come at high computational and insertion costs. As such, we investigate a proactive approach to eliminate the undesired signal response from ranges and angles of low importance by directing the energy distribution characteristics of the system.

1.1 Motivation

Current linear and planar phased array radar technologies are limited to range-independent directivity. However, this limits the radar performance to mitigate non-desirable range-dependent signal sources and thus its ability to discern targets of interests from background noise or interference. By introducing frequency diversity at the element level, we can increase the degrees of freedom in the domain space to achieve range dependent beam steering. This is realizable with the FDA concept.

Additionally, frequency diversity could be used to fulfill simultaneous mission requirements. For example, a spatial linear frequency modulation (LFM), which is simply another way of thinking about the FDA concept, could be used to image a scene while the composite signal response could be assigned to tracking or acquisition or another radar function. This is a step towards maximizing the information output by using domain diversity and again, FDA is aptly suited for this business. This is one example, and given that FDA as a topic of interest is relatively new, it is likely that possible applications are only beginning to present themselves.

1.2 Contribution

In this thesis, we extend the field of FDA research to develop efficient receiver architectures by investigating transmit and receive architectures for multiple configurations and comparing directivity responses. To begin, we investigate the uniform linear array on transmit and receive with frequency diversity at each element.

Secondly, we propose a planar array with frequency offsets along both axes such that a linear increase is witnessed in both dimensions. We also propose a receiver architecture that allows beamforming on receive to include all frequencies from a planar geometry. This will allow the receiver to maximize the signal-to-noise ratio for the available power and the signal structure herein is flexible enough to include other frequency progressions or waveform types although not investigated in this thesis.

Lastly, we present a technique designed for multi-mission, multi mode systems to use multiple beams with frequency diversity by deploying coding as a method to separate range-dependent main beam structures.

1.3 Organization

The remainder of this thesis is organized as follows. Chapter 2 contains a literature review on the topic of FDA and mentions selective publications on other relevant topics. Chapter 3 discusses receiver architectures for a linear FDA and presents the transmit and receive spatial pattern snapshots from multiple perspectives. Chapter 4, extends the linear array architectures to planar geometries and discusses the transmit and receive spatial pattern snapshots. Chapter 5 presents a multi-beam technique that enables separation of undesired main beam crossings. Lastly, Chapter 6 discusses conclusions and suggestions for future work.

Chapter 2

Literature Review

2.1 Range Dependent Transmit Spatial Pattern

The frequency diverse array (FDA) radar was first introduced in [1] as a range-dependent beamforming technique, and the transmit signal structure and associated spatial pattern theory was developed in [2]. The spatial pattern, fundamentals of which are discussed in Section 3.1, has sparked curiosity from various radar researching genres, including synthetic aperture radar (SAR) and multi-mission, multi-mode system design [3].

Born out of a desire to use waveform diversity to perform simultaneous SAR and ground moving target indication (GMTI) [1], the FDA provides a mechanism to form a range-dependent spatial beam pattern. This range-dependent beam has been described as a "bending in range" phenomenon that occurs when a frequency shift is applied from element to element across the array. They explain that the phase shift relationship between elements of the uniform linear array (ULA) yields an apparent scan angle as a function of range [2] :

$$\sin\phi^{'}(R) = \frac{2R\Delta f}{c}, \tag{2.1}$$

where Δf is the linear frequency step from element to element, R is the range and c is the speed of light. In [2], it was recognized "that some combinations of R and Δf can result in $\sin\phi^{'} > 1$. In other words, the apparent beam steer angle is outside of real space." This provides the radar designer with an additional degree of freedom and subsequently additional capability. Of course,

this is at the cost of complexity in the design of the system itself as well as other costs.

In [3], Antonik et al. suggest that by exploiting multiple degrees of freedom or domain spaces, including space, time, frequency, and modulation, and by partitioning and combining the multi-dimensional space, that waveforms can be constructed which serve multiple missions simultaneously and FDA radar seems appropriately suited achieve this goal. Patents have been issued, [4] and [5], that discussed adding degrees of freedom on the transmit waveform, namely amplitude, phase and frequency. Others have followed in furthering the transmit theory and understanding of the FDA time and range periodicity phenomenon. For example, in [6], they examined the continuous beam scanning feature in simulation and then again in [7]. In [8], the FDA, from a simulation and design perspective, was investigated and a low cost frequency diverse array design was proposed.

An extensive examination of the signal characteristics of the FDA was conducted in [9]. They performed a detailed analysis of the transmit and receive signal by investigating Doppler concerns, the ambiguity function and inter-element array spacing. Additionally, a brief examination of different waveforms and the waveform diverse array concept is presented.

2.2 SAR Using a FDA Configuration

Here-to-date, the literature has mentioned only transmit arrays or receiver architectures that reject or exclude the return signals from frequencies other than what was transmitted from that element. In [10] and [11], FDA for synthetic aperture radar purposes was investigated but they rejected signals on receive that were not frequency matched to the transmit element. These practices neglect practical considerations, such as the desire to maximize signal-to-noise, in receiver implementation and therefore motivates research to develop an architecture that does not exclude signals and extends to planar geometries.

In [10] and then in [12], they attempted to exploit FDA processing to improve SAR cross-range image resolution. The concept was to increase the angular extent of the measured scene by exploiting the bending-beam phenomenology in order to decrease the time of the imaging platform in the scene.

In [13], they were able to show, for simple point targets, that utilizing a FDA array did achieve

higher cross-range resolution for the same length synthetic aperture. However, the increase was at the cost of a higher peak-to-sidelobe ratio. Because only simple targets were used, the concept warrants further investigation to fully quantify the resolution gain achieved by this technique.

2.3 FDA in Conjunction with MIMO Radar

The FDA configuration discussed in the literature involves both the co-located and multi-static aperture arrangement. In [14], a multi-static wavelength array is introduced in which the transmit inter-element spacing is dependent on the frequency transmitted by each element. Though not depicted here, this unique pattern lessons the dependency of the range gain from angle gain and could have applications in the development of LPI (low probability of intercept) radars in range and limiting returns from undesirable ranges. This concept was further advanced in [15] to include non-linear frequency shifts. Novel beamforming techniques, for both transmit and receive, were developed in [16], but again, only the linear array was investigated.

The frequency and waveform diverse MIMO concept was first proposed in [17]. It provided a mechanism to include encryption in the transmitted waveform by merging the waveform diverse MIMO concept and FDA to increase the degrees of design freedom of an antenna array. In [16], several novel FDA beamforming techniques, and a technique for windowing on receive to limit the sidelobe structure, was summarized.

Although not completely associated with FDA, the Hybrid MIMO phased array (HMPAR) concept presented in [18] developed the basic beam patern synthesis theory for an additional FDA capable operational concept. This concept was extended in [19] to show flexibility in the choice of transmit beam patterns and investigated a related inter-pulse scanning technique.

2.4 Spurious Applications

The concept of using FDA in a multi-mission multi-mode system was first proposed in [3] as well as the concept of code diversity with FDA, this concept is investigated further in Chapter 5. This work was cited as motivation for [20], that analyzed beam paterns of chirp waveforms with slightly

different starting frequencies.

In [21] and [11] they investigated using FDA for forward-looking radar GMTI benefits. This research showed the ability of the range-dependent energy distribution characteristics of the FDA beam patern to suppress range ambiguous clutter.

Additional research on the behavior of the FDA array is presented in [22], [23], [24] to exploit the range-dependent characteristics of the FDA and the periodic nature of the beam paterns.

Chapter 3

Linear Array Receiver Architectures

We aim to design, clarify, and analyze three unique receive chain architectures to contribute insight into future system design and FDA receive pattern interpretation. In order to fully exploit the unique properties of the FDA beam pattern, the receive signal processing chain is explored for multiple configurations. Current FDA literature considers the receive signal, for a linear array, where only the transmitted frequency from each element is seen at that receive element. That is, no *bleed-through* or *cross-talk* among elements in the array is experienced. This yields a much simpler signal structure on receive and therefore simpler beamforming chain. However, as this chapter will show, this approach leaves energy and information unused, which neglects practical considerations in receiver implementation.

The remainder of this chapter is outlined as follows. Section 3.1 discusses the geometric set-up and transmit signal and spatial pattern. Section 3.1.1 investigates the time dependency of the FDA spatial pattern. Next, in section 3.2, the receive signal is developed. Section 3.3 discusses the receive architectures that are investigated. First, a band-limited coherent FDA where each element of the receiver only sees the signal that was transmitted from that element and beamforming occurs considering only that frequency. Second, full-band, pseudo-coherent FDA where each element sees all signals transmitted from each element but beamforming occurs considering only the frequency of that receive element, placing incorrect shifts for the other frequencies. Lastly, a full-band, coherent FDA architecture is investigated. In this architecture, each element sees all signals transmitted from each element and beamforming occurs matched to each frequency at each element.

We note that receive signal structures are given for each architecture, and equations associated with each are superscripted (e.g., $y^{(1)}(\cdot)$, $y^{(2)}(\cdot)$, $y^{(3)}(\cdot)$). The transmit signal is the same for all designs and therefore is not associated with a particular architecture.

3.1 FDA Transmit Pattern

A uniform 1-D linear array is discussed with spatial patterns shown in polar coordinates. We assume the radar is operating in continuous wave (CW) mode and that graphics of the patterns are snapshots for fixed time t where $t \gg \frac{2R}{c}$, $2R$ is the two-way range, and c is the speed of light. This is an important aspect of our analysis as it helps frame the approach used to describe and depict time-dependent patterns.

The elements of the array are assumed to be ideal isotropic radiators and without noise interference. For this analysis, let the array span the X-axis with inter-element spacing $d = \frac{\lambda_{min}}{2}$, and set the Y-axis as the downrange axis such that the center of the array is located at $(d\frac{N-1}{2}, 0)$, see Figure 3.1. The FDA will transmit a set of linearly increasing frequencies with step size Δf such that the set is succinctly represented as $f_n = f_c + n\Delta f$ for $n = 0...N-1$, where f_c is the carrier and N is the number of elements in the array.

The signal transmitted by the n^{th} emitter is a sinusoid given as

$$s_n(t) = \exp\{j2\pi f_n t\}. \tag{3.1}$$

The signal when delayed to a target location is

$$s_n(t) = \exp\left\{j2\pi f_n\left(t - \frac{R_n}{c}\right)\right\}. \tag{3.2}$$

The signal is measured for a target at (x_o, y_o) and element locations $(x_n, 0)$ by setting $R_n = \sqrt{(x_o - x_n)^2 + y_o^2}$. Letting the reference point be $(0, 0)$ and making a far-field approximation, we express range as $R_n \cong R_o - nd\sin\theta_o$ where $\tan\theta_o = \frac{x_o}{y_o}$ and bore-sight is measured perpendicular to the reference element along the Y-axis, see Fig 3.2.

In order to beamform on transmit, an additional phase term is necessary that comprises two

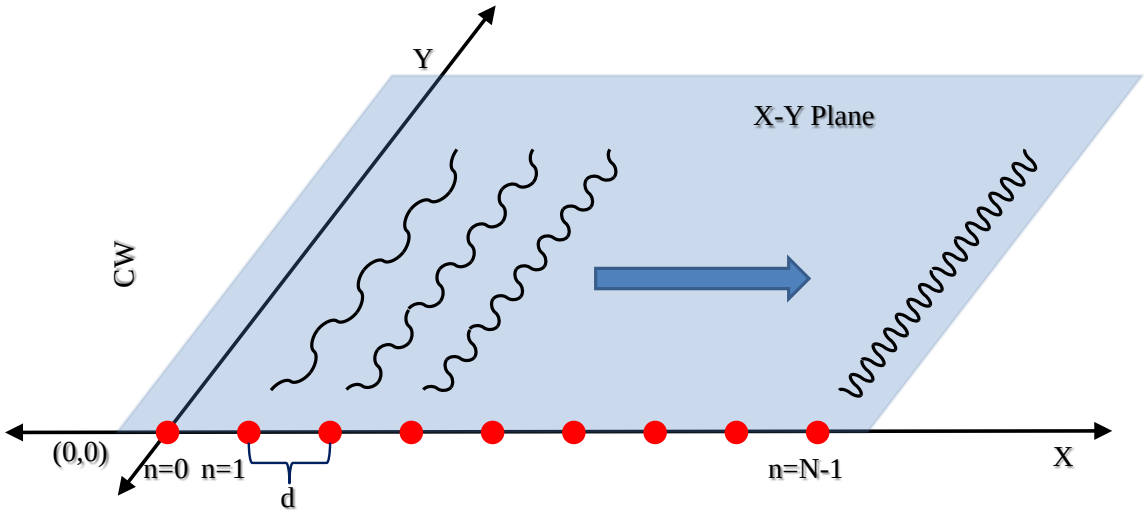

Figure 3.1: Example FDA of size $N = 9$, center located at $(d\frac{N-1}{2}, 0)$ and operating in CW mode at $f_c = 10e9$ Hz and $\Delta f = 2e3$ Hz.

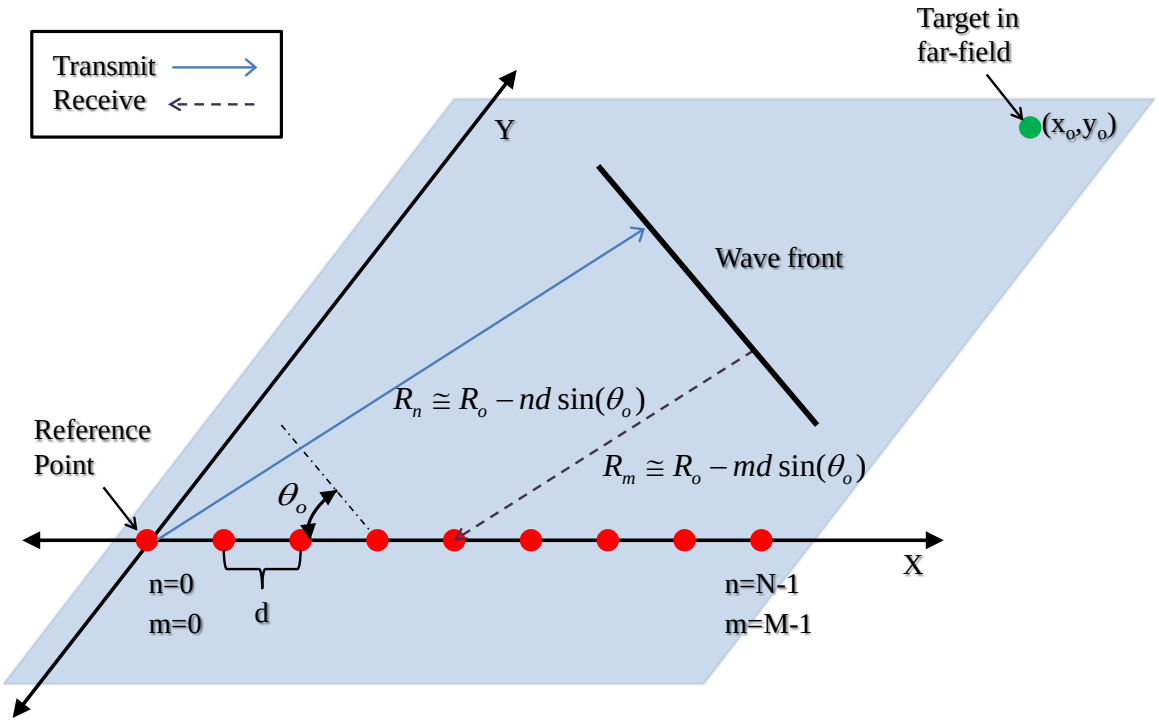

Figure 3.2: Basic geometry for a FDA of size $N = 9$, center located at $(d\frac{N-1}{2}, 0)$ and operating in CW mode at $f_c = 10e9$ Hz and $\Delta f = 2e3$ Hz.

components (angle and range). We steer the beam in angle $\hat{\theta}_o$ and range $\hat{R}_o$ to yield a composite beam-weighting factor $\alpha(\hat{R}_o, \hat{\theta}_o) = \exp\{j2\pi f_n(\frac{\hat{R}_o}{c} - \frac{nd\sin\hat{\theta}_o}{c})\}$, where $\hat{\theta}_o$ and $\hat{R}_o$ are relative to the reference element. The transmit signal from a single element as seen by a point target in space is

$$\begin{aligned} s_n(t; \hat{R}_o, \hat{\theta}_o) &= \alpha(\hat{R}_o, \hat{\theta}_o) s_n\left(t - \frac{R}{c}\right), \\ &\cong \exp\left\{j2\pi f_n\left(t - \frac{R_o}{c} + \frac{nd\sin\theta_o}{c}\right)\right\} \times \\ &\exp\left\{j2\pi f_n\left(\frac{\hat{R}_o}{c} - \frac{nd\sin\hat{\theta}_o}{c}\right)\right\}, \\ &\cong \exp\left\{j2\pi f_n\left(t - \frac{R_o - \hat{R}_o}{c} + \frac{nd(\sin\theta_o - \sin\hat{\theta}_o)}{c}\right)\right\}. \end{aligned} \tag{3.3}$$

Using this, we create the total composite signal at a point in space by summing over all elements in the ULA, given as

$$\begin{aligned} s(t; \hat{R}_o, \hat{\theta}_o) &\cong \sum_{n=0}^{N-1} \exp\left\{j2\pi f_n\left(t - \frac{R_o - \hat{R}_o}{c} + \frac{nd(\sin\theta_o - \sin\hat{\theta}_o)}{c}\right)\right\}, \\ &\cong \exp\left\{j\Phi^{(0)}\right\} \times \frac{\sin\left(\omega_f N\left(t - \frac{R_o - \hat{R}_o}{c}\right) + \omega_o N(\sin\theta_o - \sin\hat{\theta}_o)\right)}{\sin\left(\omega_f\left(t - \frac{R_o - \hat{R}_o}{c}\right) + \omega_o(\sin\theta_o - \sin\hat{\theta}_o)\right)}, \end{aligned} \tag{3.4}$$

where $\omega_f = \pi\Delta f$, $\omega_o = \frac{\pi d}{\lambda_c}$. The term $\exp\{j\Phi^{(0)}\}$ contains additional phase factors associated with the geometry of the set-up. Table 3.1 lists parameters used to simulate beam patterns under the various configurations. To give a perspective on how to interpret the patterns, a transmit spatial pattern snapshot from a FDA and a typical constant frequency (CF) array transmitting the signal in (3.4), is shown in Figure 3.3. The spatial patterns are given as power (dBw) plots, but different scaling for the transmit and receive patterns. Notice, the CF ($\Delta f = 0$) pattern has no range dependency, only azimuth, while the FDA is periodic in both range and azimuth. As expected, according to [2], we see the pattern is periodic in range every $\frac{c}{|\Delta f|} \cong \frac{3e8\frac{m}{s}}{2e3s^{-1}} = 150$ km. We also note that these simulations do not take into account mutual coupling, noise effects, non-ideal radiators or complex targets. Additionally, we assume perfect signal isolation where filters are involved. While it is possible to steer the beam strictly by modulating the offset frequency, we take the position that the Δf is fixed and that a variable phase is added at the element level to cohere at the desired coordinates.

Table 3.1: Parameters for linear array simulations

Parameter	**Value**
number TX elements N	9
number RX elements M	N
element spacing d	$\lambda_{min}/2 \cong 0.015$m
carrier frequency f_c	10 GHz
frequency offset Δf	2 kHz
range grid limits	$[0, 200]$ km
range grid spacing	1 km
azimuth grid limits	$[-90, 90]$ deg
azimuth grid spacing	1 deg
target range R_o	100 km
target azimuth θ_o	30 deg

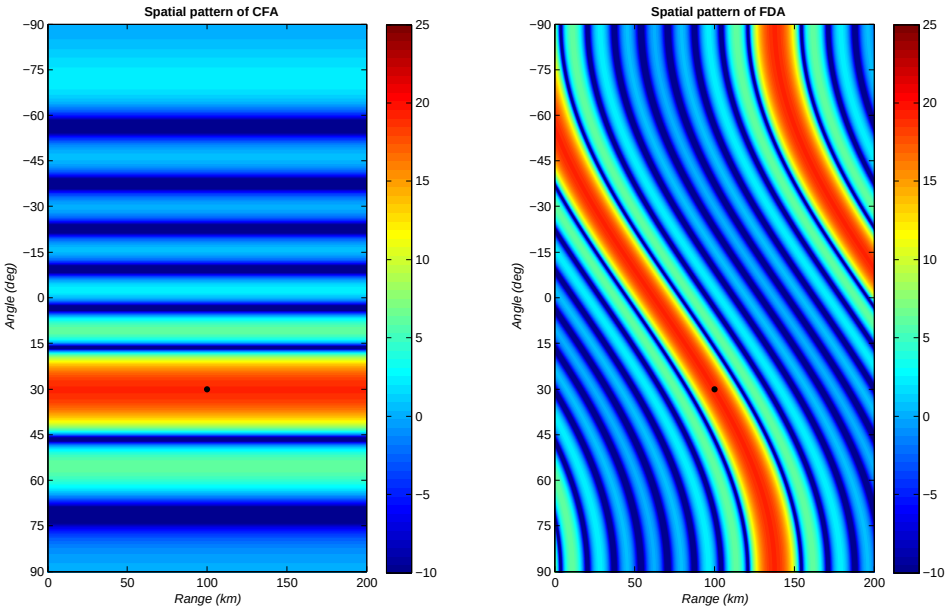

Figure 3.3: Transmit spatial patterns for a CF (left) and FD (right) array steered to target range $= 100$ km and azimuth $= 30$ deg. Target is represented as a black dot.

This adds the need for phase shifters in the design but allows additional flexibility in steering the beam.

3.1.1 FDA Time Dependency Spatial Pattern

Due to the time dependency and periodic nature of the FDA spatial patterns a brief examination of this phenomenon is warranted. As mentioned in Section 2.1 and repeated here, the FDA main beam gives an apparent scan angle equal to:

$$\sin\phi^{'}(R) = \frac{2R\Delta f}{c}. \tag{3.5}$$

This implies that for $\Delta f > 0$, the apparent scan angle will increase (scan positively) as a function of range and for $\Delta f < 0$ decrease (scan negatively) over range. It is also shown in [2] that the spatial pattern repeats itself in time as a function of the offset every $\frac{1}{|\Delta f|}$ seconds. For the parameters in Table 3.1 we show, for a period of $\frac{1}{|\Delta f|} = \frac{1}{2000} = 6.67$ μs, the spatial response broken into 8 discrete snapshots in Figure 3.4 and again for a Δf of -2 kHz in Figure 3.5. The apparent scan angle phenomenon is evident by observing the zero range main beam location in both figures. For example in Figure 3.4, it starts at about -60^o and traces positively until it repeats. The main beam also intersects the target location in Step 1 and comes back to that location again one cycle later in Step 8.

3.2 FDA Received Signal

Simplistically, the receive beamforming chain consists of a bandpass filter, phase shifter, complex weighting and power combiner. To beamform a CF array, the phase shifter applies the same linear shift across all elements because it observes only a single frequency. But, with a FDA each receive element observes different frequencies, and thus, the simplistic chain could place erroneous phase shifts, leading to inaccuracies in angle of arrival and degradation of signal-to-noise ratio (SNR).

To begin, we present the expression for a received signal at each element that has been reradiated from a single point in space. It contains the transmit and receive delays ($\frac{2R}{c}$) and the transmit

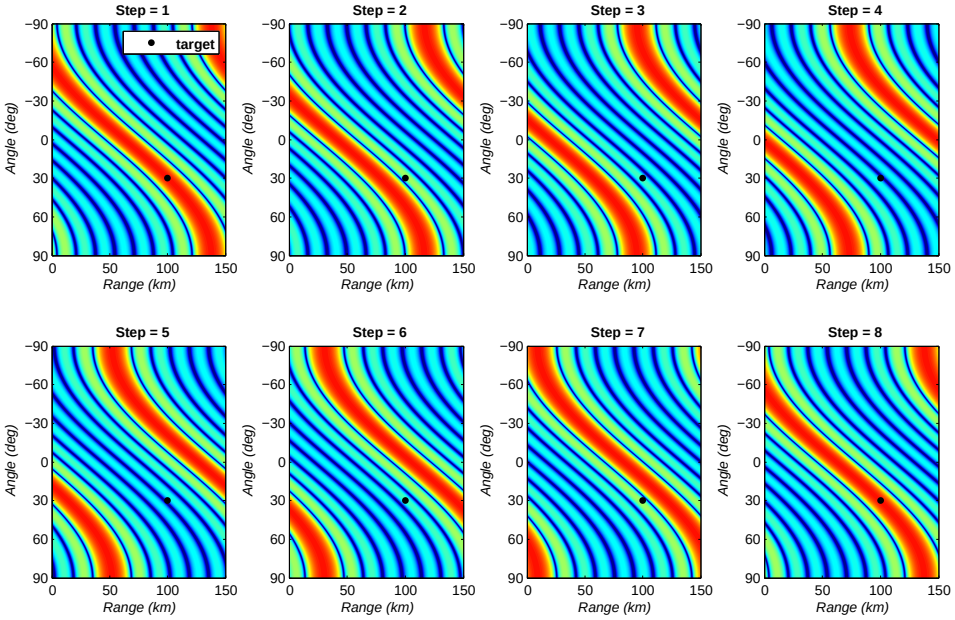

Figure 3.4: The FDA pattern is simulated for parameters in Table 5.1 and shown in 8 discrete snapshots over one periodicity (period = 6.67 μs). Target is represented as a black dot.

beam steering ($\frac{\hat{R}_o - nd\sin\hat{\theta}_o}{c}$) for N signals, yielding

$$\begin{aligned} r_m(t;\hat{R}_o,\hat{\theta}_o) &= \sum_{n=0}^{N-1} s_n\Big(t-\frac{2R}{c};\hat{R}_o,\hat{\theta}_o\Big), \\ &\cong \sum_{n=0}^{N-1} \exp\left\{ j2\pi f_n \left(t - \frac{2R_o}{c} + \frac{\hat{R}_o}{c} + \right.\right. \\ &\left.\left. \frac{nd(\sin\theta_o - \sin\hat{\theta}_o)}{c} + \frac{md\sin\theta_o}{c} \right) \right\}, \end{aligned} \tag{3.6}$$

where the number of transmit and receive elements are the same.

Using this signal, we investigate three processing chains. The following sections include block diagrams and the spatial patterns for each architecture, where the goal for each chain is to put the maximum possible signal at the target location.

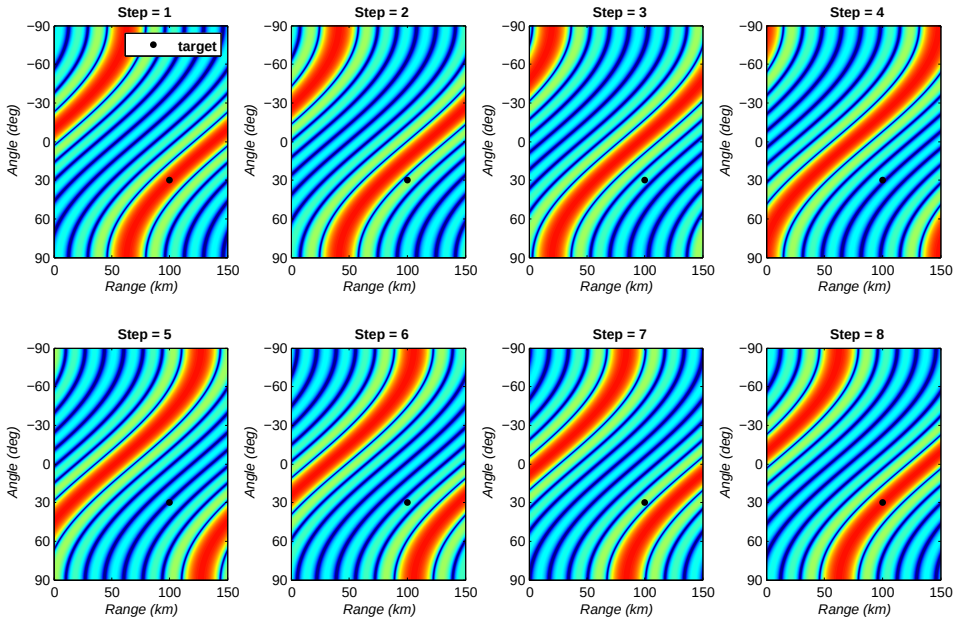

Figure 3.5: The FDA pattern is simulated for parameters in Table 5.1, except $\Delta f = -2000$ Hz, and shown in 8 discrete snapshots over one periodicity (period = 6.67 μs). Target is represented as a black dot.

3.3 Receiver Processing Architectures

3.3.1 Band-limited, Coherent FDA

The band-limited, coherent FDA architecture is the method with the least component changes from the CF receive chain mentioned above. Figure 3.6 depicts a block diagram of the receive chain where filter $h_m^{(1)}$ has bandwidth only to capture the tone of interest. This ensures no cross-talk at the element level and thus the beamformer phase shift is applied correctly to that frequency. The filter is modeled simply by omitting any response from frequencies other than what was transmitted from that element. The single-channel filtered signal is, for a single point in space,

$$\begin{aligned} v_m^{(1)}(t;\hat{R}_o,\hat{\theta}_o) &= h_m^{(1)}\{r_m(t;\hat{R}_o,\hat{\theta}_o)\}, \\ &\cong \exp\left\{ j2\pi f_m \left(t - \frac{2R_o}{c} + \frac{\hat{R}_o}{c} + \frac{2md\sin\theta_o}{c} - \frac{md\sin\hat{\theta}_o}{c} \right) \right\}. \end{aligned} \tag{3.7}$$

Using the filtered signal, we compose the complete received signal for a single point in space, with the complex beamforming weights $\beta_m^{(1)}(\hat{R}_o, \hat{\theta}_o) = \exp\{j2\pi f_m(\frac{\hat{R}_o}{c} - \frac{md\sin\hat{\theta}_o}{c})\}$. This signal is

$$\begin{aligned} y^{(1)}(t;\hat{R}_o,\hat{\theta}_o) &= \sum_{m=0}^{N-1} \beta_m^{(1)}(\hat{R}_o,\hat{\theta}_o) v_m^{(1)}(t;\hat{R}_o,\hat{\theta}_o), \\ &\cong \sum_{m=0}^{N-1} \exp\left\{ j2\pi f_m \left(t - \frac{2(R_o - \hat{R}_o)}{c} + \frac{2md(\sin\theta_o - \sin\hat{\theta}_o)}{c} \right) \right\}, \\ &\cong \exp\left\{ j\Phi^{(1)} \right\} \times \\ &\frac{\sin\left(\omega_f N\left(t - 2\frac{R_o - \hat{R}_o}{c}\right) + 2\omega_o N(\sin\theta_o - \sin\hat{\theta}_o) \right)}{\sin\left(\omega_f\left(t - 2\frac{R_o - \hat{R}_o}{c}\right) + 2\omega_o(\sin\theta_o - \sin\hat{\theta}_o) \right)}. \end{aligned} \tag{3.8}$$

The term $\exp\{j\Phi^{(1)}\}$ contains additional phase factors associated with the geometry of the set-up. These delays comprise the total two-way delay for a beam steered on transmit and receive but not matched to the appropriate receive channel. This is the familiar receive signal structure and spatial pattern used for analysis in [11, 16, 24] where a closed-form expression of this architecture can also be found. In Figure 3.7, we use the signal in (3.8) to achieve a representation of the composite receive spatial pattern. Analyzing this pattern, we see the periodicity of the pattern is halved in range, given that the elapsed time is now a two-way concern. An additional receive pattern artifact of the FDA structure are the ambiguities in range and angle that manifest. This could be an issue of great concern for a system designer. However, possible ambiguity resolution techniques are not addressed.

While this configuration correctly forms a FDA beam, it grossly degrades the SNR by blocking energy transmitted from other elements. Additionally, if possible to exploit, the limited spatial information in the other signals is also lost.

3.3.2 Full-band, Pseudo-coherent FDA

Utilizing the beamforming chain in Figure 3.8, we define filter $h^{(2)}$ as having bandwidth wide enough to capture all transmitted signals with equal weight, and we proceed to form the receive signal structure again with beamforming. The transmit structure is unchanged, but in this architecture, all the signals are observed by each receive element. However, the phase applied at each element is

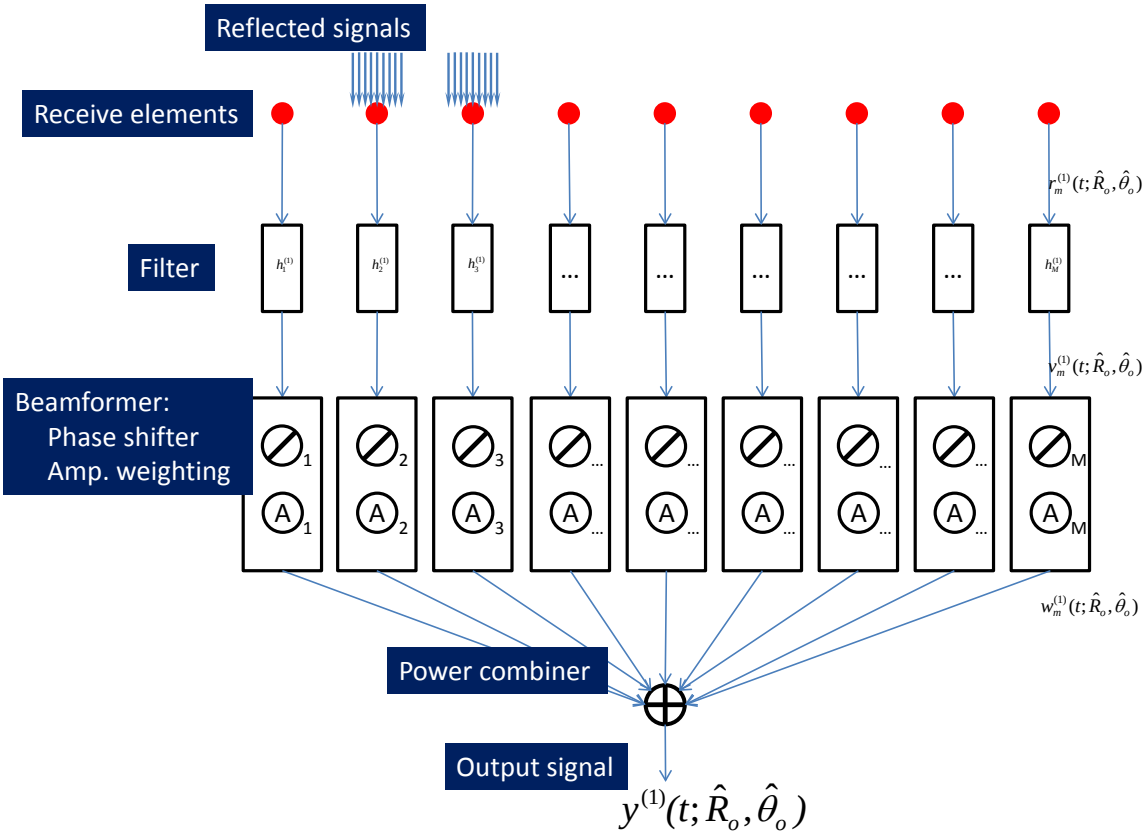

Figure 3.6: Simplistic beamforming chain for the band-limited, coherent FDA architecture. Including narrowband filter, complex weighting mechanism and power combiner.

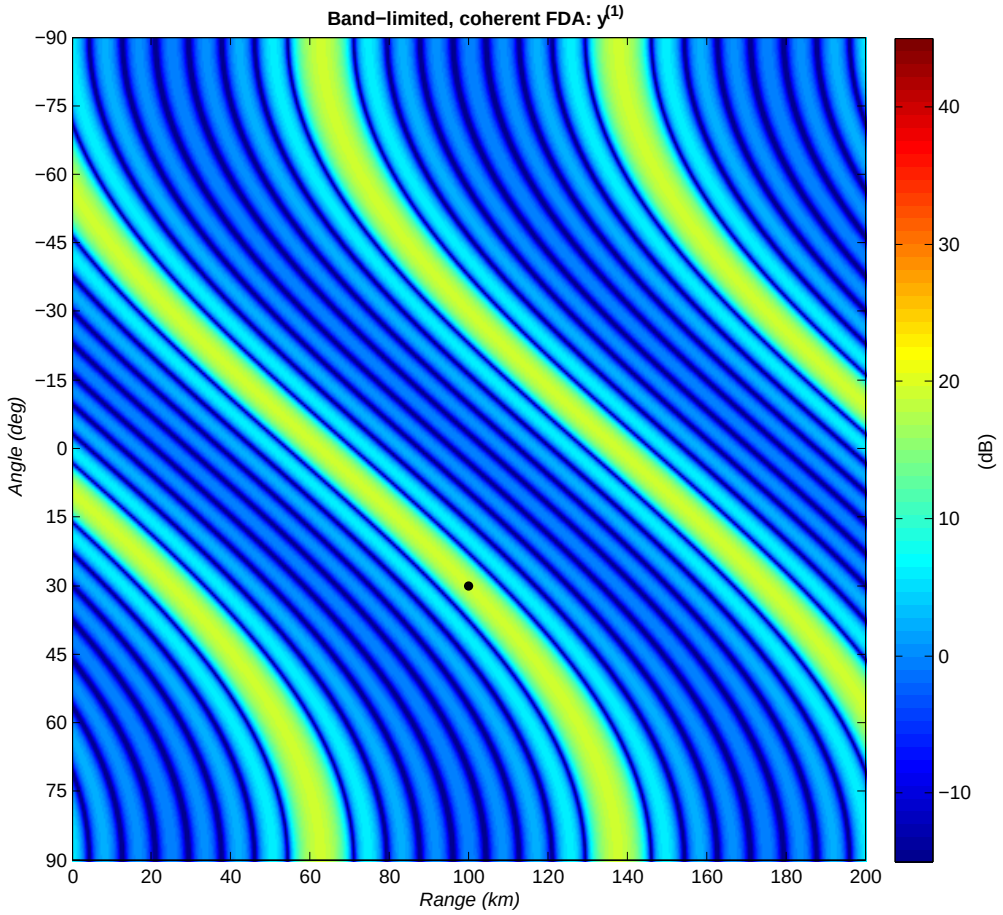

Figure 3.7: The composite receive pattern is shown for the band-limited, coherent FDA architecture using signal $y^{(1)}$ in (3.8). The steering position is represented by a black dot.

steering-matched only to the tone transmitted from that element, hence pseudo-coherent. Cross-talk is thus present among the elements, but the potential for error is also present, as the correct steering phase shift is frequency dependent. The receive signal filtered by $h^{(2)}$ is

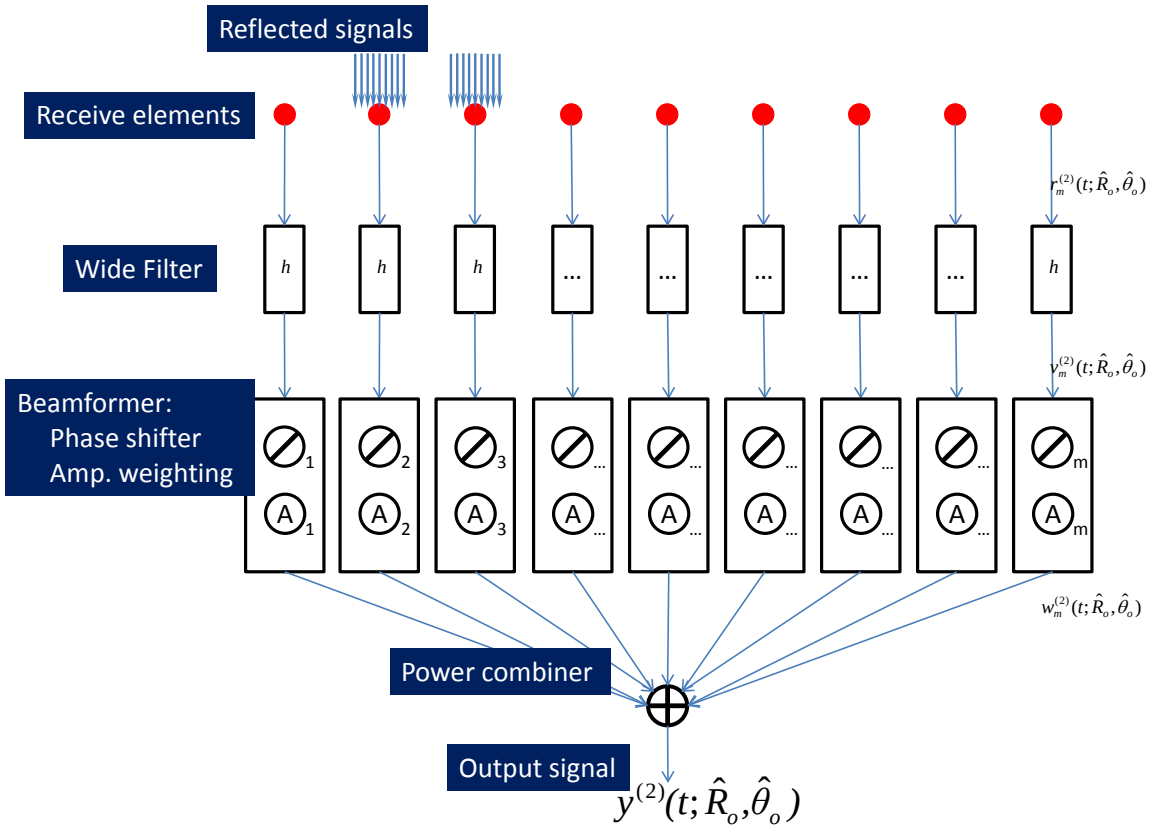

Figure 3.8: Beamforming chain for the full-band, pseudo-coherent FDA architecture. Including wideband filter, complex weighting mechanism and power combiner.

$$
\begin{aligned}
v_m^{(2)}(t;\hat{R}_o,\hat{\theta}_o) &= h^{(2)}\{r_m(t;\hat{R}_o,\hat{\theta}_o)\}, \\
&= r_m(t;\hat{R}_o,\hat{\theta}_o), \\
&\cong \sum_{n=0}^{N-1} \exp\left\{ j2\pi f_n \left(t - \frac{2R_o}{c} + \frac{\hat{R}_o}{c} + \right.\right. \\
&\left.\left. \frac{nd(\sin\theta_o - \sin\hat{\theta}_o)}{c} + \frac{md\sin\theta_o}{c} \right) \right\}.
\end{aligned}
\tag{3.9}
$$

Using the filtered signal, we can compose the complete received signal for a single point in space, with the beamforming component $\beta_m^{(2)}(\hat{R}_o, \hat{\theta}_o) = \exp\{j2\pi f_m(\frac{\hat{R}_o}{c} - \frac{md\sin\hat{\theta}_o}{c})\}$ as

$$\begin{aligned} y^{(2)}(t;\hat{R}_o,\hat{\theta}_o) &= \sum_{m=0}^{N-1}\sum_{n=0}^{N-1}\beta_m^{(2)}(\hat{R}_o,\hat{\theta}_o)v_m^{(2)}(t;\hat{R}_o,\hat{\theta}_o), \\ &\cong \sum_{m=0}^{N-1}\sum_{n=0}^{N-1}\exp\left\{j2\pi f_n\left(t-\frac{2R_o}{c}+\frac{\hat{R}_o}{c}+\frac{nd(\sin\theta_o-\sin\hat{\theta}_o)}{c}+\right.\right. \\ &\left.\left.\frac{md\sin\theta_o}{c}\right)\right\}\times\exp\left\{j2\pi f_m\left(\frac{\hat{R}_o}{c}-\frac{md\sin\hat{\theta}_o}{c}\right)\right\}, \\ &\cong \exp\left\{j\Phi^{(2)}\right\}\times\frac{\sin\left(\omega_f N\frac{\hat{R}_o}{c}+\omega_o N(\sin\theta_o-\sin\hat{\theta}_o)\right)}{\sin\left(\omega_f\frac{\hat{R}_o}{c}+\omega_o(\sin\theta_o-\sin\hat{\theta}_o)\right)}\times \\ &\frac{\sin\left(\omega_f N\left(t-\frac{2R_o}{c}+\frac{\hat{R}_o}{c}\right)+\omega_o N(\sin\theta_o-\sin\hat{\theta}_o)\right)}{\sin\left(\omega_f\left(t-\frac{2R_o}{c}+\frac{\hat{R}_o}{c}\right)+\omega_o(\sin\theta_o-\sin\hat{\theta}_o)\right)}, \end{aligned} \tag{3.10}$$

where $\exp\{j\Phi^{(2)}\}$ contains terms due to the geometric set-up. Comparing this result to (3.8), the only difference is the inclusion of terms in the sum for $m \neq n$. A snapshot of the resulting composite receive spatial pattern is presented in Figure 3.9. Using this design, all of the received energy is used, but the main beam is not steered to the target location in the final stage of beamforming due to unaccounted for cross-talk.

3.3.3 Full-band, Coherent FDA

The full-band, coherent FDA architecture is the most efficient receiver design of the three presented. This configuration observes all frequencies at each element and has a filter bank that enables the correct phase shift for each frequency and element to be applied. By correct phase shift, we mean the shift required to cohere energy from each transmit element being received on any receive element such that the maximum signal is at the target. We note that the only goal of this beamformer is to achieve maximum signal at the target location, not preserve any other phenomenon of the FDA pattern.

Figure 3.10 gives an example set-up where each filter bank H_m contains N narrowband filters h_n with weighting hardware associated with only that frequency if received at that element. In this set-up, all signals are matched perfectly, and no energy or information is lost. The notation for this

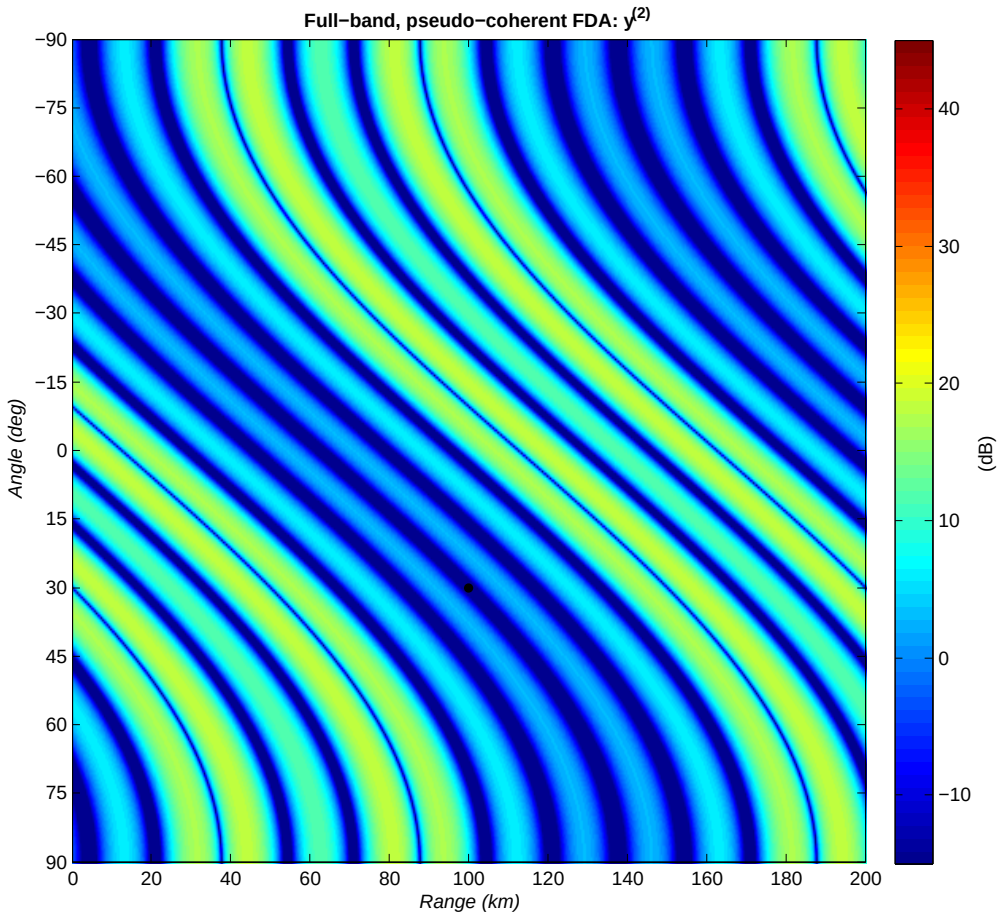

Figure 3.9: The composite receive pattern is shown for the full-band, pseudo-coherent FDA architecture using signal $y^{(2)}$ in (3.10). The steering position is represented by a black dot.

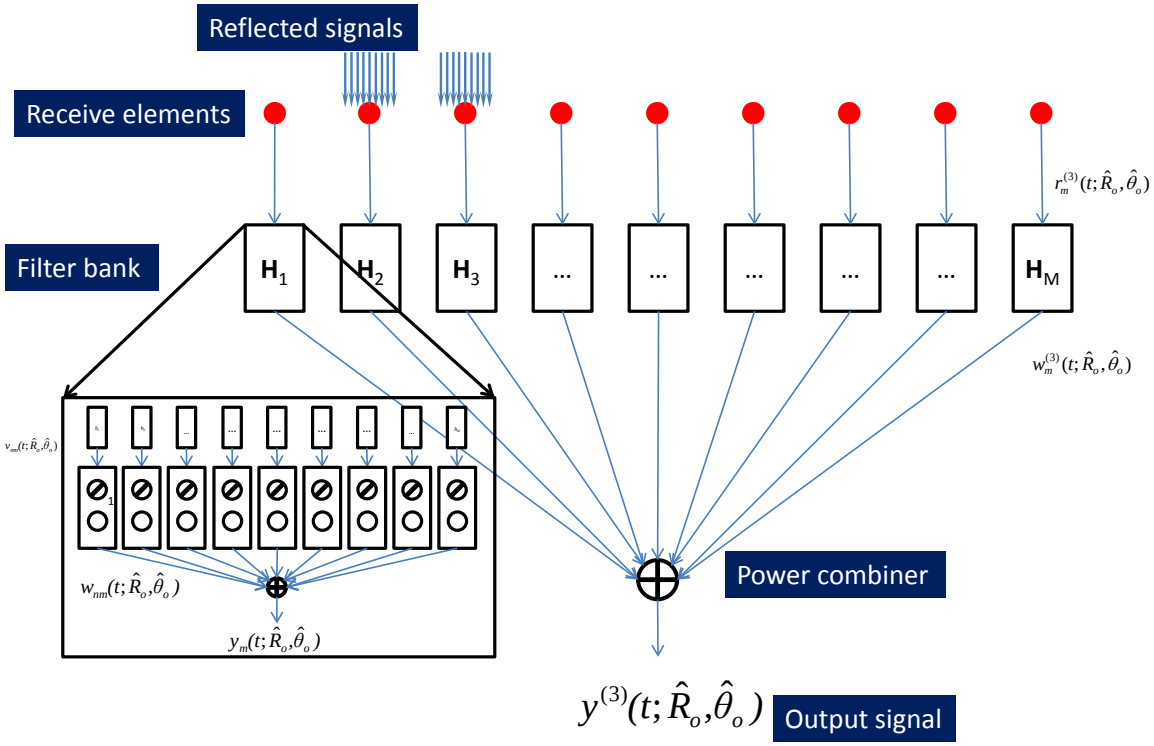

Figure 3.10: Beamforming chain for the full-band, coherent FDA architecture. Including filter banks at each receive element that apply appropriate phase shifts to steer the beam in range and angle.

architecture is slightly different due to the additional components that are introduced. To begin, the transmit signal $s_n(t;\hat{R}_o,\hat{\theta}_o)$ is unchanged, and the received signal $r_m(t;\hat{R}_o,\hat{\theta}_o)$ enters the filter bank H_m. The signal output by the n^{th} filter h_{nm} at the m^{th} receive element is

$$\begin{aligned} v_{nm}(t;\hat{R}_o,\hat{\theta}_o) &= h_{nm}\{r_m(t;\hat{R}_o,\hat{\theta}_o)\}, \\ &\cong \exp\left\{ j2\pi f_n \left(t - \frac{2R_o}{c} + \frac{\hat{R}_o}{c} + \right.\right. \\ &\left.\left. \frac{nd(\sin\theta_o - \sin\hat{\theta}_o)}{c} + \frac{md\sin\theta_o}{c} \right) \right\}. \end{aligned} \tag{3.11}$$

Continuing, the filtered and beam-weighted signal out of the n^{th} beamformer at the m^{th} receive element is given as

$$\begin{aligned} w_{nm}(t;\hat{R}_o,\hat{\theta}_o) &= \beta_{nm}(\hat{R}_o,\hat{\theta}_o) v_{nm}(t;\hat{R}_o,\hat{\theta}_o), \\ &\cong \exp\left\{ j2\pi f_n \left(t - \frac{2(R_o - \hat{R}_o)}{c} + \frac{nd(\sin\theta_o - \sin\hat{\theta}_o)}{c} + \right.\right. \\ &\left.\left. \frac{md(\sin\theta_o - \sin\hat{\theta}_o)}{c} \right) \right\}, \end{aligned} \tag{3.12}$$

where $\beta_{nm}(\hat{R}_o,\hat{\theta}_o) = \exp\{j2\pi f_n(\frac{\hat{R}_o}{c} - \frac{md\sin\hat{\theta}_o}{c})\}$. The last component of the filter bank stage is the combiner, where the output is given as

$$\begin{aligned} y_m(t;\hat{R}_o,\hat{\theta}_o) &= \sum_{n=0}^{N-1} w_{nm}(t;\hat{R}_o,\hat{\theta}_o), \\ &\cong \sum_{n=0}^{N-1} \exp\left\{ j2\pi f_n \left(t - \frac{2(R_o - \hat{R}_o)}{c} + \frac{nd(\sin\theta_o - \sin\hat{\theta}_o)}{c} + \right.\right. \\ &\left.\left. \frac{md(\sin\theta_o - \sin\hat{\theta}_o)}{c} \right) \right\}. \end{aligned} \tag{3.13}$$

At this point in the beamforming, we are exiting the filter bank stage, and all that remains is to combine the signals from all filter banks. The composite signal is computed as a sum over M receivers of signals from N transmitters that have been delayed out and back ($\frac{2R}{c}$) from a target, steered on transmit ($\frac{\hat{R}_o - nd\sin\hat{\theta}_o}{c}$) and then steered on receive by matching the frequency f_n with the

appropriate steering associated with each receive element m to yield

$$\begin{aligned} y^{(3)}(t;\hat{R}_o,\hat{\theta}_o) &= \sum_{m=0}^{N-1} y_m(t,\hat{R}_o,\hat{\theta}_o), \\ &\cong \sum_{m=0}^{N-1}\sum_{n=0}^{N-1} \exp\left\{ j2\pi f_n \left(t - \frac{2(R_o-\hat{R}_o)}{c} + \right.\right. \\ &\left.\left. \frac{nd(\sin\theta_o - \sin\hat{\theta}_o)}{c} + \frac{md(\sin\theta_o - \sin\hat{\theta}_o)}{c} \right) \right\}. \end{aligned} \tag{3.14}$$

In order to generate a closed-form expression, we assume narrow bandwidth operation (i.e. $n\Delta f \ll f_c$). In doing so, the terms $(\frac{\Delta f n^2 d(\sin\theta_o - \sin\hat{\theta}_o)}{c})$ and $(\frac{\Delta f nmd(\sin\theta_o - \sin\hat{\theta}_o)}{c})$ that manifest when multiplying out can be dropped as they are negligible. Recognizing (3.14) is a familiar geometric series and applying Euler's formula, we achieve the $\frac{\sin(Nx)}{\sin(x)}$ structure with additional factors in front associated with the geometry abbreviated here as $\Phi^{(3)}$ in the following

$$\begin{aligned} y^{(3)}(t;\hat{R}_o,\hat{\theta}_o) \cong \exp\left\{ j\Phi^{(3)} \right\} \times \\ \frac{\sin\left(\omega_o N(\sin\theta_o - \sin\hat{\theta}_o)\right)}{\sin\left(\omega_o(\sin\theta_o - \sin\hat{\theta}_o)\right)} \times \\ \frac{\sin\left(\omega_f N(t - 2\frac{R_o-\hat{R}_o}{c}) + \omega_o N(\sin\theta_o - \sin\hat{\theta}_o)\right)}{\sin\left(\omega_f(t - 2\frac{R_o-\hat{R}_o}{c}) + \omega_o(\sin\theta_o - \sin\hat{\theta}_o)\right)}. \end{aligned} \tag{3.15}$$

The signal in (3.15) is used to generate the composite receive spatial pattern in Figure 3.11. It also contains range and angle dependent sidelobe structures, but this beamformer achieves maximum signal on target.

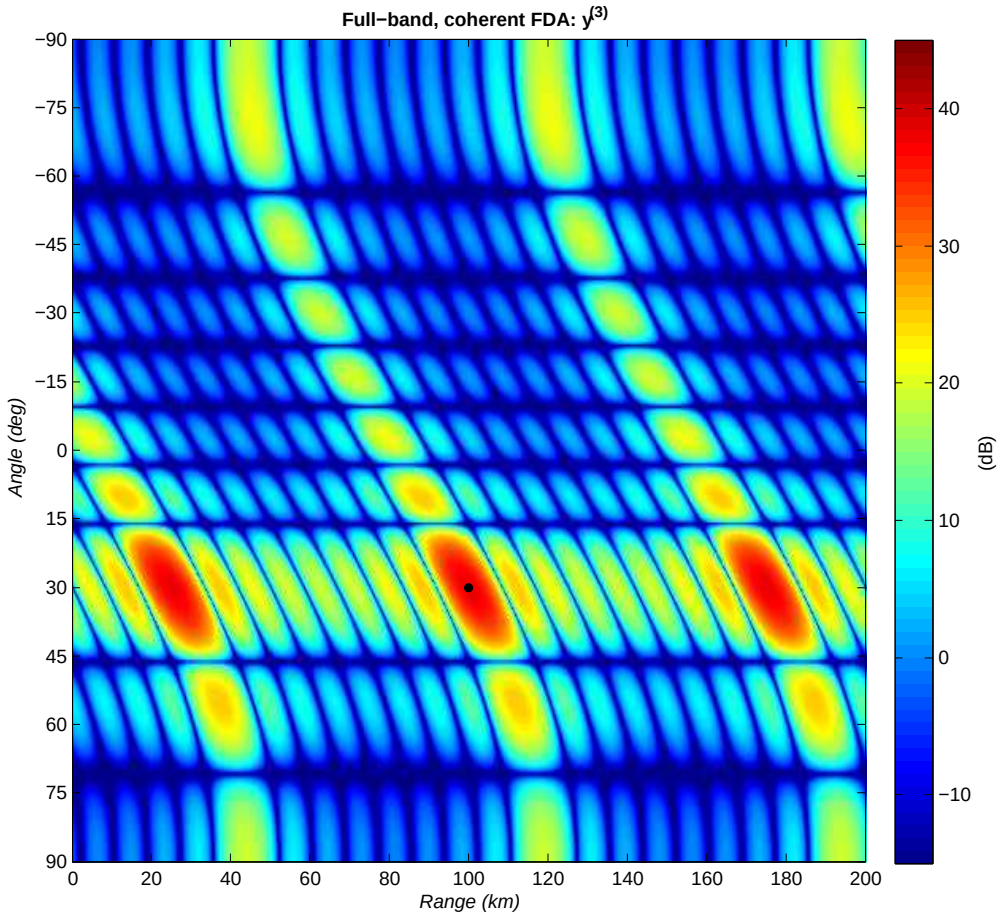

Figure 3.11: The composite receive pattern is shown for the full-band, coherent FDA architecture using signal $y^{(3)}$ in (3.14). The steering position is represented by a black dot and this configuration places maximum signal at that location.

Chapter 4

Planar Array Architectures

Frequency diverse array radar systems have future use in multi-mission, multi-mode structures, as suggested in [3]. Specifically, when the energy distribution requirements of a radar would benefit from a controllable range dependency, the FDA architecture would satiate this need. Much has been investigated regarding the linear frequency diverse (FD) array, but many radar applications require the ability to beamsteer in higher dimensionalities than a linear array affords, prompting the planar array development suggested in this chapter.

Typically, planar array systems allow beamsteering in two dimensions (azimuth and elevation) but is range independent. This requires additional signal processing to determine the range of a target of interest. FDA systems allow for three-dimensional beamsteering with a planar array geometry and could possibly lead to elimination of additional range processing, although that is not discussed here.

The remainder of this chapter is outlined as follows. Section 4.1 discusses the geometry and scenario, including parameters used for simulation. Section 4.2 develops the transmit signal structure, gives a closed-form expression of the spatial patterns after making a narrowband approximation, and charts the transmit spatial pattern when compared to a standard CF array. Section 4.3 develops the receiver architecture and spatial pattern.

4.1 Geometry and Scenario

The elements of the planar FDA are assumed to be ideal isotropic radiators and without noise interference. For this analysis, again let the array span the X-axis with inter-element spacing $d_x = \frac{\lambda_{min}}{2}$, and Y-axis with inter-element spacing $d_y = \frac{\lambda_{min}}{2}$, such that the reference element of the array is located at $(0, 0, 0)$, and λ_{min} corresponds to the wavelength of the maximum frequency transmitted by the array, see Figure 4.1. In this chapter, the FDA will transmit a set of linearly increasing frequencies, on the X and Y-axes with step sizes $\Delta f_x = \Delta f$ and $\Delta f_y = (N+1)\Delta f$, respectively, where $|\Delta f|$ is limited in order for the system to be considered narrowband. Doing so, the set is succinctly represented as $f_{nm} = f_c + n\Delta f_x + m\Delta f_y$ for $n = 0...N-1$ and $m = 0...M-1$, where f_c is the carrier and N and M are the number of elements in the array along the X and Y-axes, respectively. In the manner of [**?**], see Figure 4.2 for a graphical depiction of this configuration.

We assume the radar is operating in continuous wave (CW) mode and that graphics of the patterns are snapshots for fixed time t where $t \gg \frac{2R}{c}$, $2R$ is the two-way range, and c is the RF speed of propagation. However, it must be remembered that FDA spatial patterns are periodic in time.

In the following receiver architecture discussion, we note that linear frequency progression on either axis is not necessary, but it does require complete spectral diversity, meaning no repeated frequencies on transmit. Without this spectral diversity to distinguish each signal on receive, an additional method, such as coding, would be necessary to separate the signals to apply the appropriate beamforming weights.

In the following two sections, the transmit and receive signals are developed and simulated using the parameters found in Table 4.1. It provides values for quantifiable parameters such as, the number of elements in the array, the grid limits, grid spacing for the points in space where the signal was calculated and measured, as well as the target location.

4.2 Planar FDA Transmit Pattern

In this section, we discuss the complete transmit signal, present a closed-form expression for the planar transmit spatial pattern, and graphically depict the shape of the main beam spatial pattern.

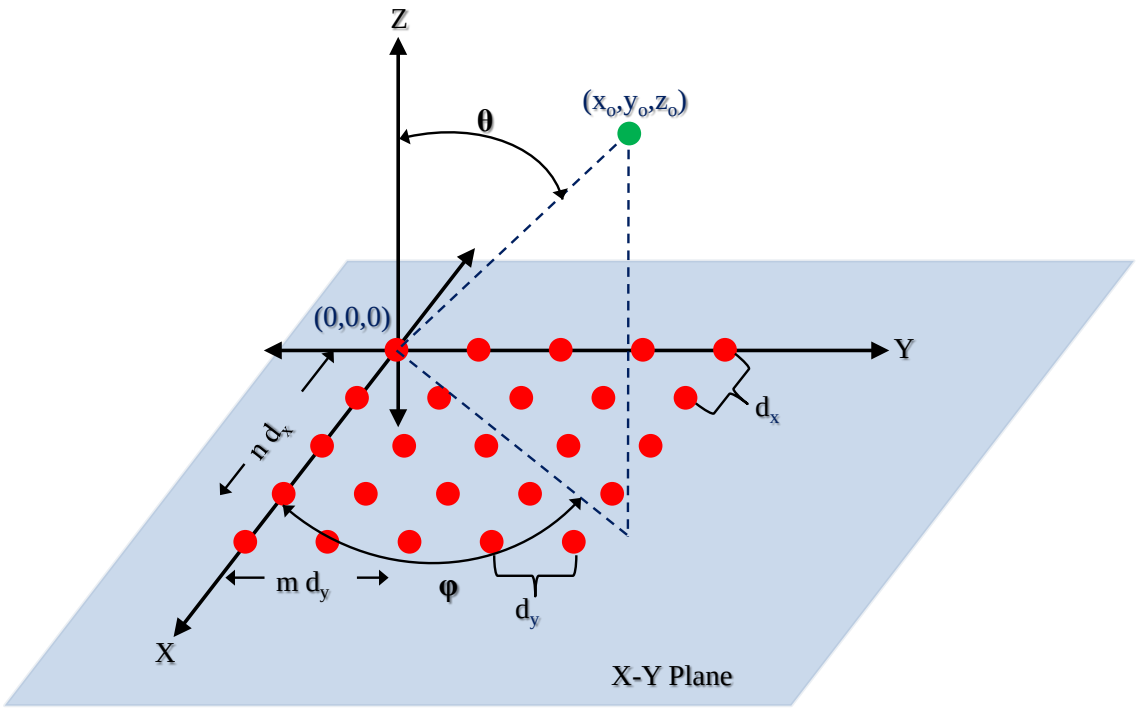

Figure 4.1: Basic geometry for a planar FDA with reference point at $(0, 0, 0)$ and target at (x_o, y_o, z_o).

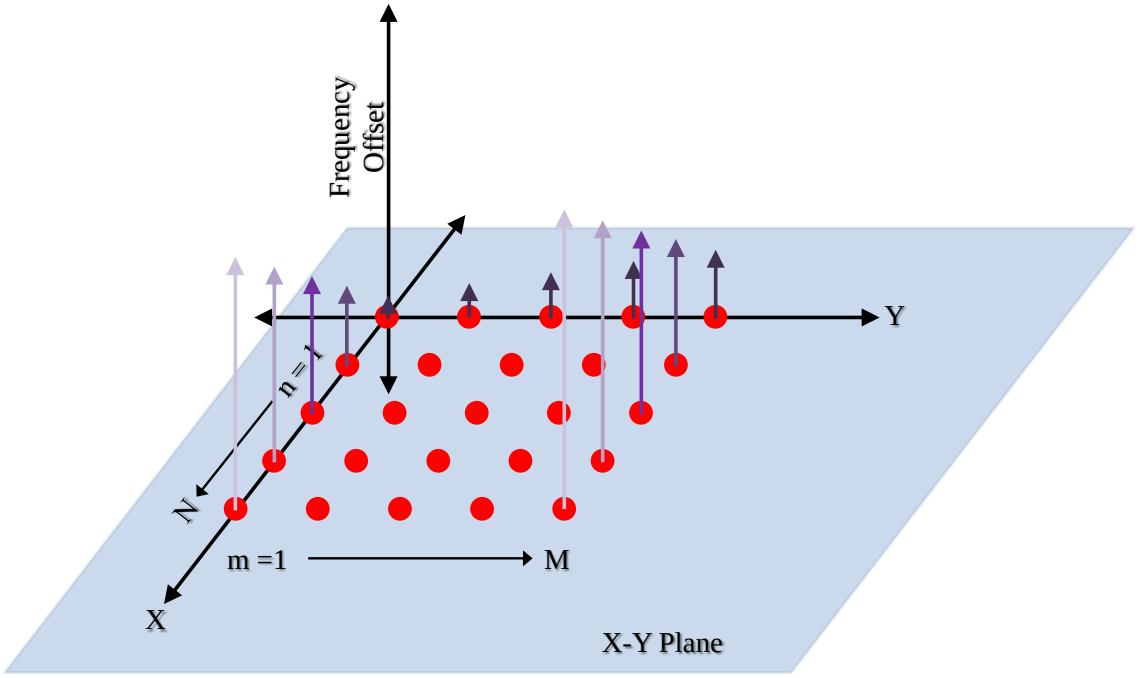

Figure 4.2: Example of planar FDA with equal inter-element spacing on both axis, such that element $(1, 1)$ is located at the origin and the array progresses along the positive X and Y-axes, respectively.

Table 4.1: Parameters for planar array parameters

Parameter	Value
number X-axis elements: N	9
number Y-axis elements: M	9
element spacing: d_x and d_y	$\lambda_{min}/2 \cong 0.015$m
carrier frequency: f_c	10 GHz
X-axis frequency offset: Δf_x	1 kHz
Y-axis frequency offset: Δf_y	10 kHz
X grid limits	$[-100, 100]$ km
X grid spacing	2 km
Y grid limits	$[-100, 100]$ km
Y grid spacing	2 km
Z grid limits	$[0, 200]$ km
Z grid spacing	2 km
target X location: x_o	0 km
target Y location: y_o	0 km
target Z location: z_o	100 km

4.2.1 Transmit Signal Model

The signal transmitted by the (n, m) emitter is a sinusoid given as

$$s_{nm}(t) = \exp\{j2\pi f_{nm} t\}. \tag{4.1}$$

The signal when delayed to a target location is

$$s_{nm}(t) = \exp\left\{j2\pi f_{nm}\left(t - \frac{R_{nm}}{c}\right)\right\}. \tag{4.2}$$

The signal is measured for a target at (x_o, y_o, z_o) for element locations $(x_n, y_m, 0)$ by setting $R_{nm} = \sqrt{(x_o - x_n)^2 + (y_o - y_m)^2 + z_o^2}$. Letting the reference point be $(0, 0, 0)$ and making a far-field approximation, we express range as

$$R_{nm} \cong R_o - nd_x \sin\theta_o \cos\phi_o - md_y \sin\theta_o \sin\phi_o, \tag{4.3}$$

where $R_o = \sqrt{x_o^2 + y_o^2 + z_o^2}$, $\cos\theta_o = \frac{z_o}{R_o}$ and $\tan\phi_o = \frac{y_o}{x_o}$, and boresight is measured perpendicular to the reference element along the Z-axis (see Figure 4.1). This allows (4.2) to be rewritten

as

$$s_{nm}(t) \cong \exp\left\{ j2\pi f_{nm}\left(t - \frac{R_o}{c} + \frac{nd_x \sin\theta_o \cos\phi_o}{c} + \frac{md_y \sin\theta_o \sin\phi_o}{c} \right) \right\}. \tag{4.4}$$

In order to beamform on transmit, an additional phase term is necessary that comprises two components (angle and range). We steer the beam in angle ($\hat{\theta}_o$, $\hat{\phi}_o$) and range $\hat{R}_o$ to yield a composite beam-weighting factor

$$\alpha(\hat{R}_o, \hat{\theta}_o, \hat{\phi}_o) = \exp\left\{ j2\pi f_{nm}\left(\frac{\hat{R}_o}{c} - \frac{nd_x \sin\hat{\theta}_o \cos\hat{\phi}_o}{c} - \frac{md_y \sin\hat{\theta}_o \sin\hat{\phi}_o}{c} \right) \right\}, \tag{4.5}$$

where ($\hat{\theta}_o$, $\hat{\phi}_o$) and $\hat{R}_o$ are relative to the reference element. The transmit signal from a single element as seen by a point target in space is

$$\begin{aligned} s_{nm}(t; \hat{R}_o, \hat{\theta}_o, \hat{\phi}_o) &= \alpha(\hat{R}_o, \hat{\theta}_o, \hat{\phi}_o) s_{nm}\left(t - \frac{R_{nm}}{c} \right), \\ &= \exp\left\{ j2\pi f_{nm}\left(t - \frac{R_o - \hat{R}_o}{c} + \right.\right. \\ &\quad \frac{nd_x(\sin\theta_o \cos\phi_o - \sin\hat{\theta}_o \cos\hat{\phi}_o)}{c} \\ &\quad \left.\left. + \frac{md_y(\sin\theta_o \sin\phi_o - \sin\hat{\theta}_o \sin\hat{\phi}_o)}{c} \right) \right\}. \end{aligned} \tag{4.6}$$

Continuing, consider the transmit signal in (4.6) from each element and sum over all X and Y-axes contributions to give the total observed signal at (x_o, y_o, z_o):

$$\begin{aligned} s(t; \hat{R}_o, \hat{\theta}_o, \hat{\phi}_o) &= \sum_{n=0}^{N-1} \sum_{m=0}^{M-1} \alpha(\hat{R}_o, \hat{\theta}_o, \hat{\phi}_o) s_{nm}\left(t - \frac{R_{nm}}{c} \right), \\ &= \sum_{n=0}^{N-1} \sum_{m=0}^{M-1} \exp\left\{ j2\pi f_{nm}\left(t - \frac{R_o - \hat{R}_o}{c} + \right.\right. \\ &\quad \frac{nd_x(\sin\theta_o \cos\phi_o - \sin\hat{\theta}_o \cos\hat{\phi}_o)}{c} \\ &\quad \left.\left. + \frac{md_y(\sin\theta_o \sin\phi_o - \sin\hat{\theta}_o \sin\hat{\phi}_o)}{c} \right) \right\}. \end{aligned} \tag{4.7}$$

$$s(t;\hat{R}_o,\hat{\theta}_o,\hat{\phi}_o) \cong \exp\left\{j\Phi_{nm}\right\}\times \\ \frac{\sin\left(\omega_x N\left(t-\frac{R_o-\hat{R}_o}{c}\right)+\omega_{o_x}N(\sin\theta_o\cos\phi_o-\sin\hat{\theta}_o\cos\hat{\phi}_o)\right)}{\sin\left(\omega_x\left(t-\frac{R_o-\hat{R}_o}{c}\right)+\omega_{o_x}(\sin\theta_o\cos\phi_o-\sin\hat{\theta}_o\cos\hat{\phi}_o)\right)} \\ \times\frac{\sin\left(\omega_y M\left(t-\frac{R_o-\hat{R}_o}{c}\right)+\omega_{o_y}M(\sin\theta_o\sin\phi_o-\sin\hat{\theta}_o\sin\hat{\phi}_o)\right)}{\sin\left(\omega_y\left(t-\frac{R_o-\hat{R}_o}{c}\right)+\omega_{o_y}(\sin\theta_o\sin\phi_o-\sin\hat{\theta}_o\sin\hat{\phi}_o)\right)}, \tag{4.8}$$

Making a plane wave approximation (target range, $R \gg \frac{D^2}{4\lambda_{min}}$, D is largest dimension of aperture) and narrowband assumption (bandwidth $\ll f_c$) we derive a closed-form expression where $\omega_x = \pi\Delta f_x, \omega_{o_x} = \frac{\pi d_x}{\lambda_c}, \omega_y = \pi\Delta f_y, \omega_{o_y} = \frac{\pi d_y}{\lambda_c}$ and $\lambda_c = \frac{c}{f_c}$. The term $\exp\{j\Phi_{nm}\}$ contains additional phase factors associated with the geometry of the set-up, but do not necessarily contribute to the structure of the pattern, which is of most importance. It is important to note that by making the narrowband assumption and manipulating the signal into a sinc-like structure, we are excluding the quadratic phase terms that manifest when multiplying out the frequency components.

4.2.2 Planar Array Spatial Pattern Snapshot

In Figure 4.3, we display the 10-dB main beam width. While sidelobes are present, they are greater than 10-dB down from the main beam and therefore are not visible in this portrayal. To get a better feel for the iso-surface presentation [25], observe the cross section of the CF transmit spatial pattern and notice the concentric rings of varying color that represent receding gain values. As expected, the CF pattern does not vary spatially but the FDA pattern appears periodic in angle and range in three dimensions. Additionally, we display the patterns of four different offset configurations in Figures 4.4, 4.5, 4.6, 4.7. Notice that even though the offsets can have the same magnitude, the pattern is also dictated by the "direction" of the offset $(+,-)$ and along which axis (X,Y) the offset progresses. In the following figures we are visualizing a single pattern ambiguity, if we computed the pattern for a larger volume, the periodicity would be evident. This phenomenon could be a nuisance for the radar designer, but with range fall-off and selective frequency offset choices such that the ambiguities are below the minimum discernible signal of the system, it could be an uncontroversial point.

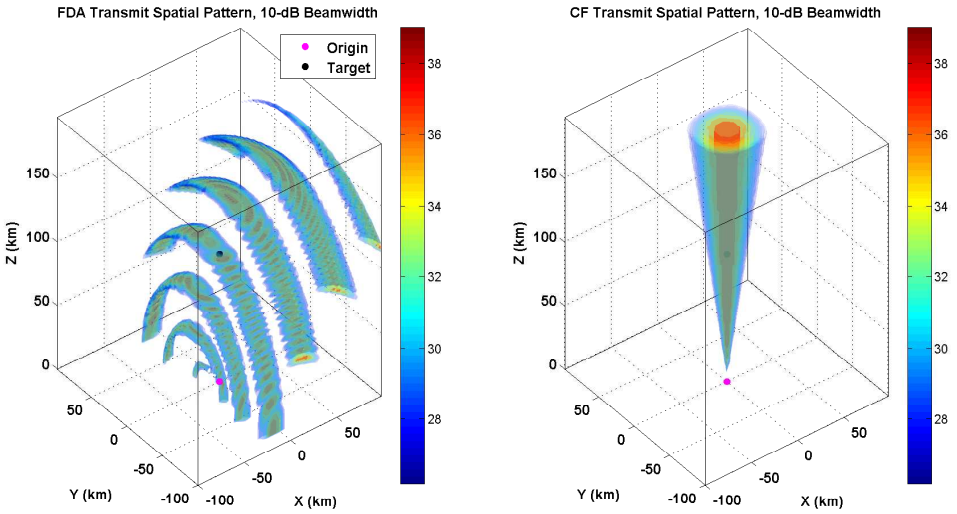

Figure 4.3: The 10-dB main beam transmit pattern is shown for a 9×9 planar array with (left) frequency diversity ($\Delta f_x = 1$ kHz, $\Delta f_y = 10$ kHz) and (right) constant frequency transmit waveforms.

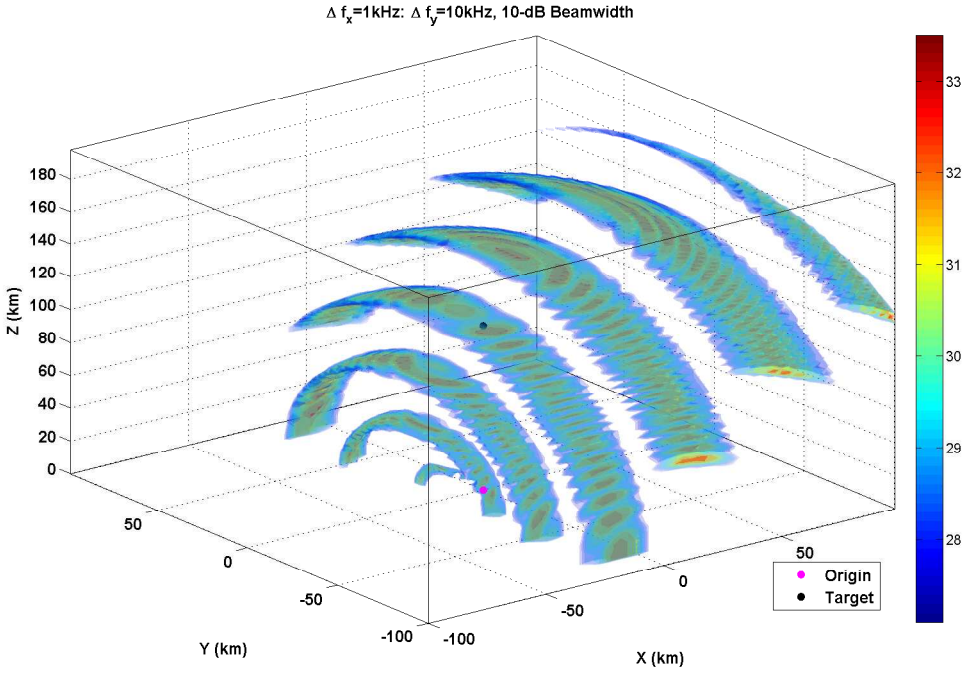

Figure 4.4: Transmit spatial pattern snapshot from a planar FDA radar for different frequency offsets. $\Delta f_x = 1$ kHz, $\Delta f_y = 10$ kHz

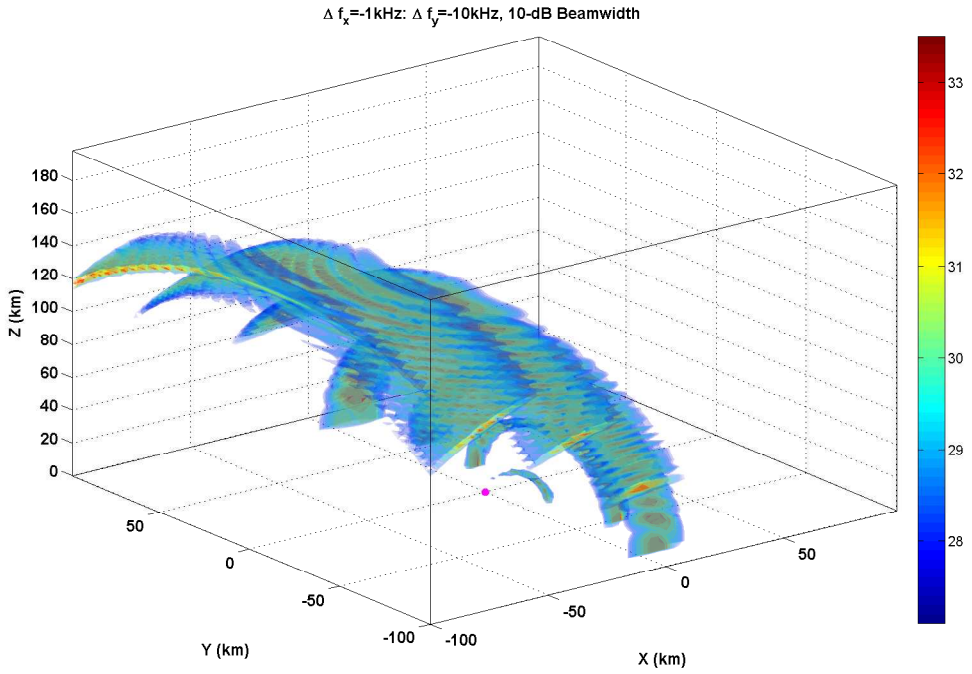

Figure 4.5: Transmit spatial pattern snapshot from a planar FDA radar for different frequency offsets. $\Delta f_x = -1$ kHz, $\Delta f_y = -10$ kHz

4.3 Planar FDA Receive Pattern

We now develop the receive architecture and signal structure and provide a 4-D visualization of the main beam receive spatial pattern.

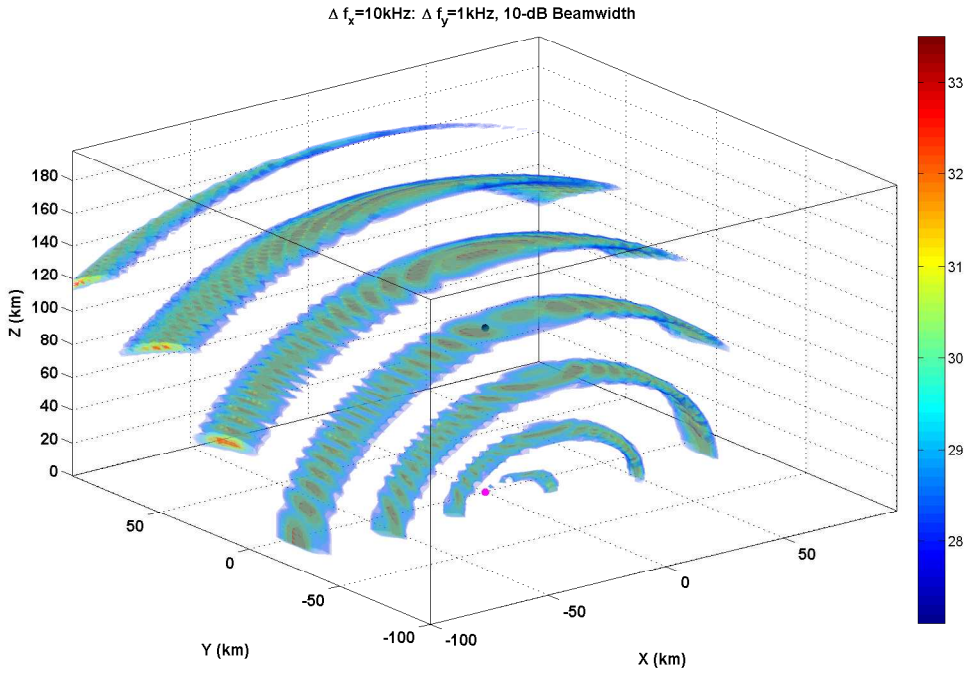

Figure 4.6: Transmit spatial pattern snapshot from a planar FDA radar for different frequency offsets. $\Delta f_x = 10$ kHz, $\Delta f_y = 1$ kHz

4.3.1 Receive Signal Model

Begin with the complete transmit signal in (4.7) and account for the two-way delay to arrive at the received signal at each node

$$\begin{aligned} y_{pq}(t) &= \sum_{n=0}^{N-1}\sum_{m=0}^{M-1} \alpha(\hat{R}_o, \hat{\theta}_o, \hat{\phi}_o) s_{nm}\left(t - \frac{R_{nm} + R_{pq}}{c}\right), \\ &\cong \sum_{n=0}^{N-1}\sum_{m=0}^{M-1} \exp\left\{ j2\pi f_{nm}\left(t - \frac{2R_o - \hat{R}_o}{c} + \right.\right. \\ &\frac{nd_x(\sin\theta_o\cos\phi_o - \sin\hat{\theta}_o\cos\hat{\phi}_o)}{c} + \frac{md_y(\sin\theta_o\sin\phi_o - \sin\hat{\theta}_o\sin\hat{\phi}_o)}{c} + \\ &\left.\left. \frac{pd_x\sin\theta_o\cos\phi_o}{c} + \frac{qd_y\sin\theta_o\sin\phi_o}{c}\right)\right\}. \end{aligned} \tag{4.9}$$

In order to apply the appropriate phase to each frequency and reconstruct to beamform, it is necessary to filter at each receive element to parse the received signal according to its transmitting node. We then apply the beamform weighting and combine to form the final output. Figure 4.8 shows the

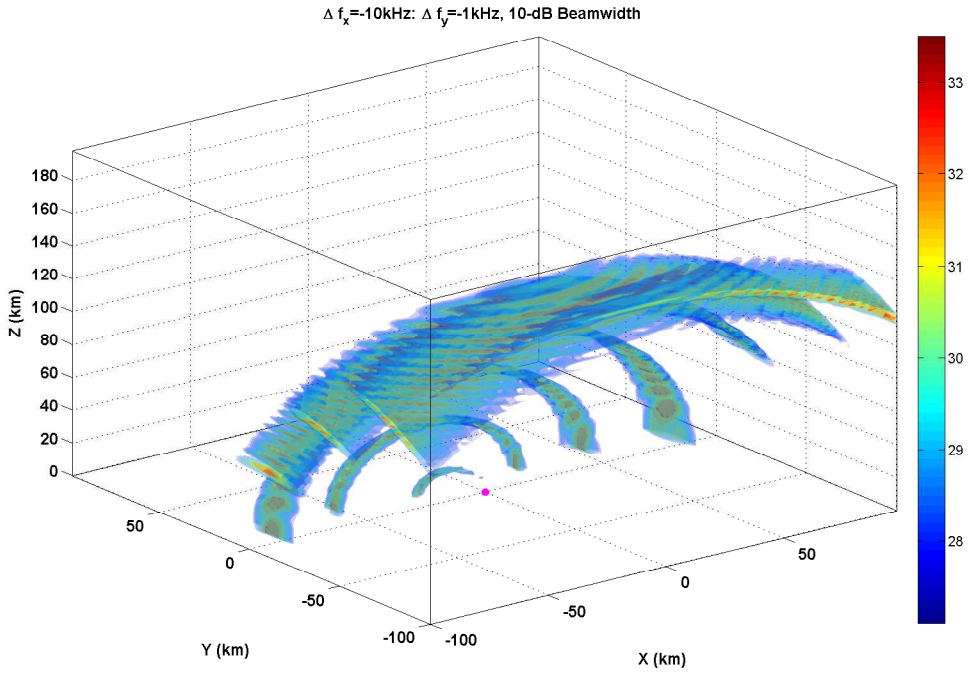

Figure 4.7: Transmit spatial pattern snapshot from a planar FDA radar for different frequency offsets. $\Delta f_x = -10$ kHz, $\Delta f_y = -1$ kHz

architecture necessary to complete the reconstruction. The additional signal labels are for intermediate steps that, for convenience and succinctness, are not discussed. However, for a more complete derivation of a uniform linear array see [26]. The beamforming weight is

$$\beta_{pqnm}(\hat{R}_o, \hat{\theta}_o, \hat{\phi}_o) = \exp\left\{ j2\pi f_{nm} \left(\frac{\hat{R}_o}{c} - \frac{p d_x \sin\hat{\theta}_o \cos\hat{\phi}_o}{c} - \frac{q d_y \sin\hat{\theta}_o \sin\hat{\phi}_o}{c} \right) \right\}, \tag{4.10}$$

such that the beamformed received signal is expressed as

$$y(t; \hat{R}_o, \hat{\theta}_o, \hat{\phi}_o) = \sum_{p=0}^{P-1} \sum_{q=0}^{Q-1} \sum_{n=0}^{N-1} \sum_{m=0}^{M-1} \exp\left\{ j2\pi f_{nm} \left(t - \frac{2(R_o - \hat{R}_o)}{c} + \frac{(n+p) d_x (\sin\theta_o \cos\phi_o - \sin\hat{\theta}_o \cos\hat{\phi}_o)}{c} + \frac{(m+q) d_y (\sin\theta_o \sin\phi_o - \sin\hat{\theta}_o \sin\hat{\phi}_o)}{c} \right) \right\}. \tag{4.11}$$

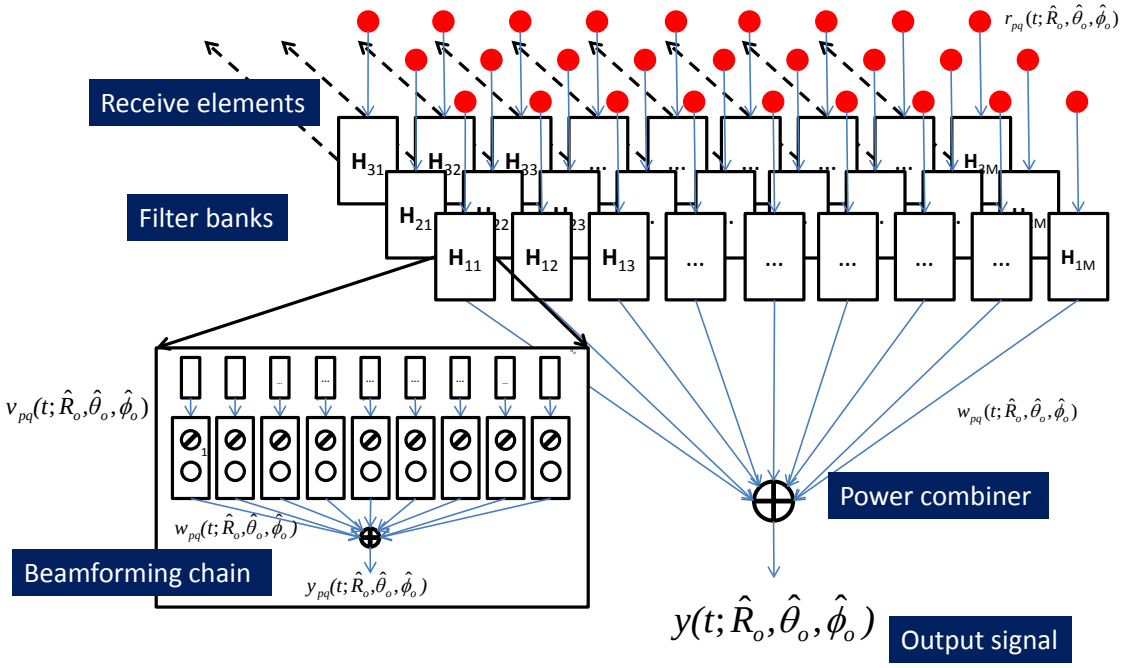

Figure 4.8: Receive beamforming chain of the planar FDA architecture. Including filter banks at each receive node that apply appropriate phase shifts to steer the beam in range and angle for a planar array.

Maintaining the assumptions of a plane wave and narrowband signal on receive, we arrive at a closed-form expression given as

$$
\begin{aligned}
y(t;\hat{R}_o,\hat{\theta}_o,\hat{\phi}_o) \cong \exp\left\{j\Psi\right\} &\times \frac{\sin\left(\omega_{o_p}P(\sin\theta_o\cos\phi_o-\sin\hat{\theta}_o\cos\hat{\phi}_o)\right)}{\sin\left(\omega_{o_p}(\sin\theta_o\cos\phi_o-\sin\hat{\theta}_o\cos\hat{\phi}_o)\right)} \\
&\times \frac{\sin\left(\omega_{o_q}Q(\sin\theta_o\sin\phi_o-\sin\hat{\theta}_o\sin\hat{\phi}_o)\right)}{\sin\left(\omega_{o_q}(\sin\theta_o\sin\phi_o-\sin\hat{\theta}_o\sin\hat{\phi}_o)\right)} \\
&\times \frac{\sin\left(\omega_x N\left(t-\frac{R_o-\hat{R}_o}{c}\right)+\omega_{o_x}N(\sin\theta_o\cos\phi_o-\sin\hat{\theta}_o\cos\hat{\phi}_o)\right)}{\sin\left(\omega_x\left(t-\frac{R_o-\hat{R}_o}{c}\right)+\omega_{o_x}(\sin\theta_o\cos\phi_o-\sin\hat{\theta}_o\cos\hat{\phi}_o)\right)} \\
&\times \frac{\sin\left(\omega_y M\left(t-\frac{R_o-\hat{R}_o}{c}\right)+\omega_{o_y}M(\sin\theta_o\sin\phi_o-\sin\hat{\theta}_o\sin\hat{\phi}_o)\right)}{\sin\left(\omega_y\left(t-\frac{R_o-\hat{R}_o}{c}\right)+\omega_{o_y}(\sin\theta_o\sin\phi_o-\sin\hat{\theta}_o\sin\hat{\phi}_o)\right)},
\end{aligned}
\tag{4.12}
$$

where $\omega_{o_p}=\frac{\pi d_x}{\lambda_c}$, $\omega_{o_q}=\frac{\pi d_y}{\lambda_c}$ and $\exp\{j\Psi\}$ contains additional phase factors associated with the geometry of the set-up.

4.3.2 Spatial Pattern Snapshots

In Figure 4.9, the 4-D composite transmit and receive spatial pattern snapshot is shown for 10-dB off the peak value. Notice that the main beam does not have as simple a pattern as the transmitter. Of importance to note is that the composite receive signal does not match the structure of the transmit pattern. This is due to the fact that the transmit and receive patterns are not the same. The objective of this receiver architecture is to cohere energy at the steered location, not preserve any other attribute of the pattern. While other configurations are available, they are not investigated here. Again, we are visualizing a single pattern ambiguity, if we computed the pattern for a larger volume the periodicity would be evident.

The FDA pattern in Figures 4.9, 4.10, and 4.11 shows that, in this configuration, the main beam no longer traces out a spiral in space but is simply surrounding the target area. The volume around the target is the 10-dB beamwidth of the main beam on receive. While it appears that energy is only around the target, sidelobe energy is present but not visible. Figures 4.12, 4.13, 4.14, and 4.15 further investigate this by allowing the beamwidth to increase in consecutive plots by 5-dB at a

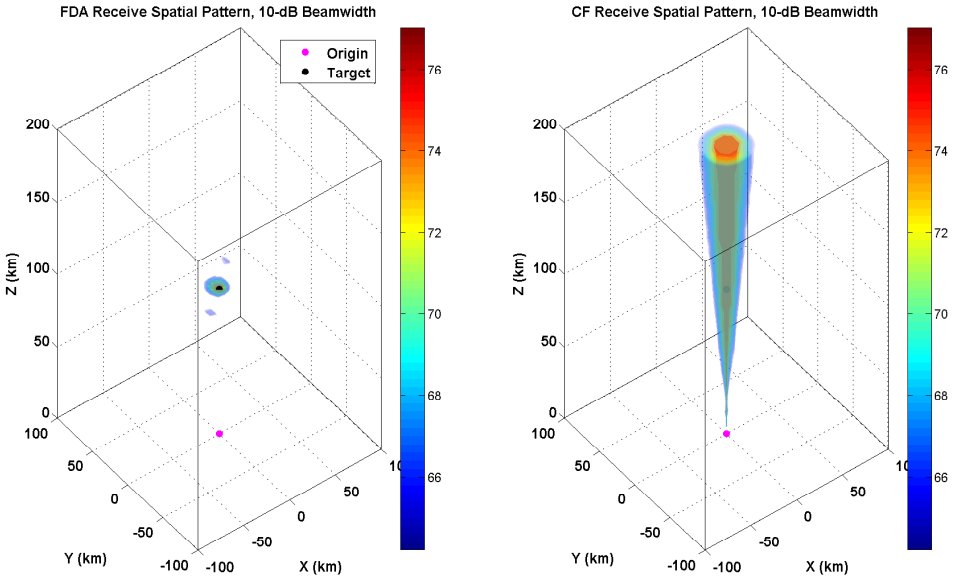

Figure 4.9: The 10-dB receive pattern structure snapshot is shown for a 9×9 planar array with (left) frequency diversity and (right) constant frequency transmit waveforms. Global view.

time. As we increase the beamwidth that is visualized, more of the sidelobe structure of the pattern becomes apparent.

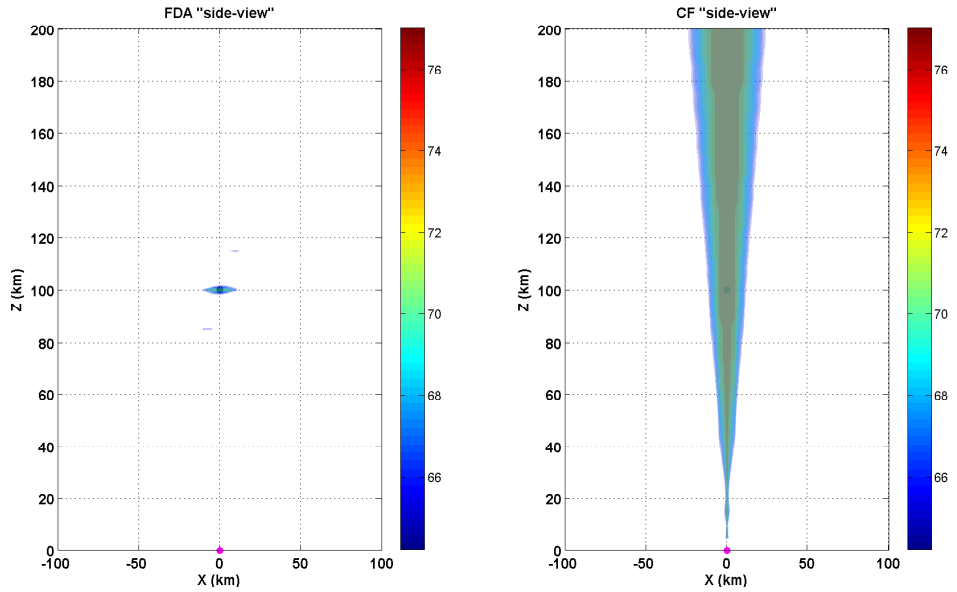

Figure 4.10: The 10-dB receive pattern structure snapshot is shown for a 9×9 planar array with (left) frequency diversity and (right) constant frequency transmit waveforms. Side view.

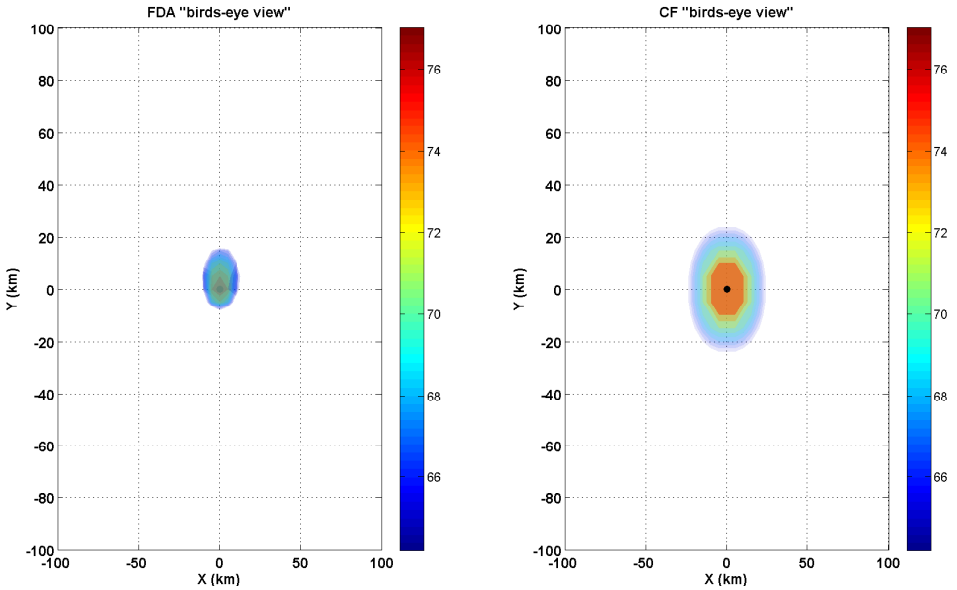

Figure 4.11: The 10-dB receive pattern structure snapshot is shown for a 9×9 planar array with (left) frequency diversity and (right) constant frequency transmit waveforms. Top view.

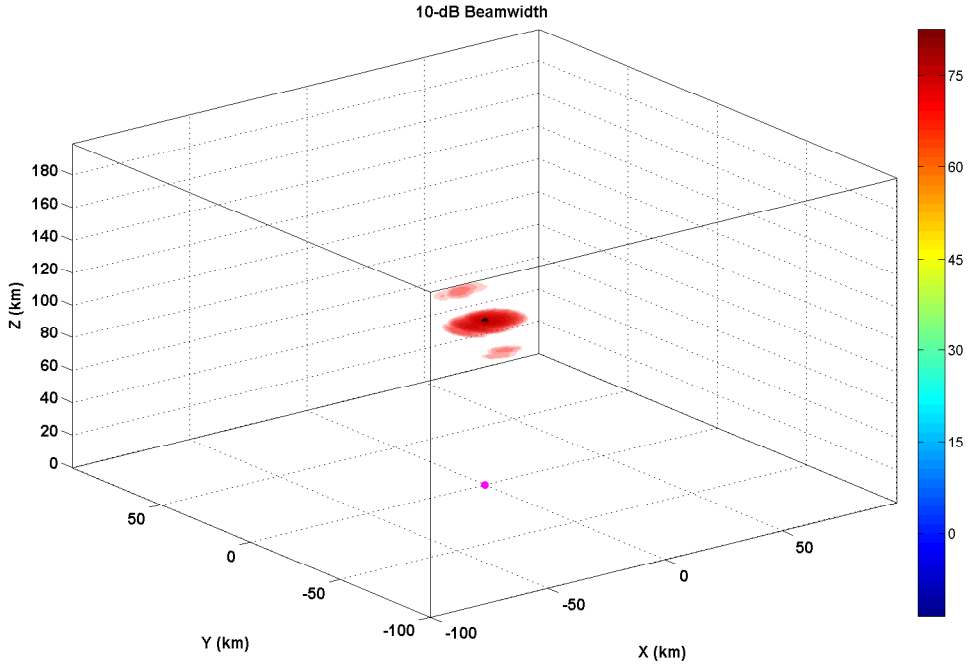

Figure 4.12: Composite receive pattern snapshot for a 9×9 FDA for 10-dB beamwidth.

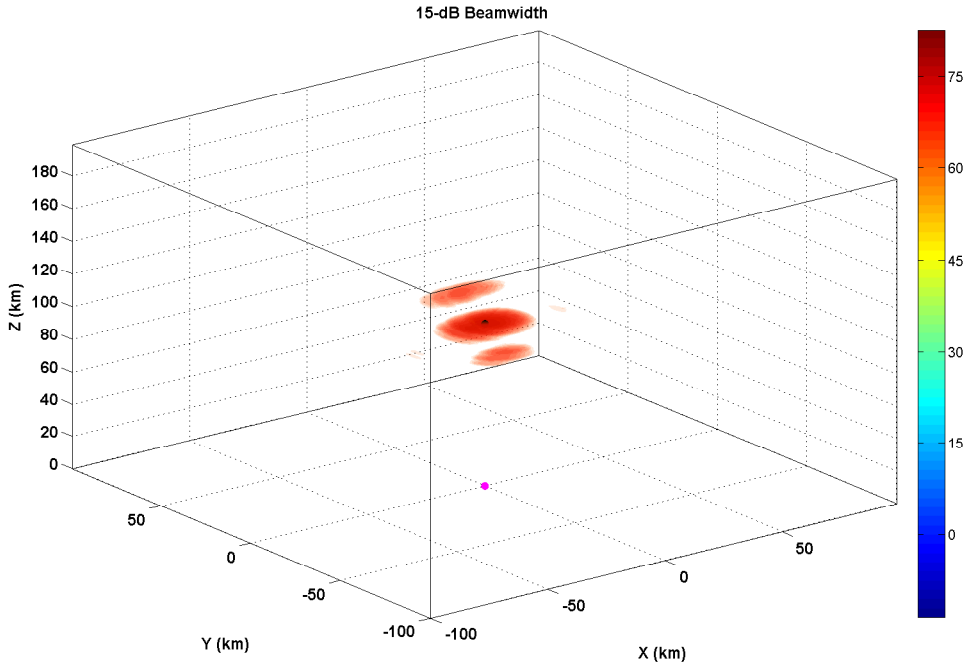

Figure 4.13: Composite receive pattern snapshot for a 9×9 FDA for 15-dB beamwidth.

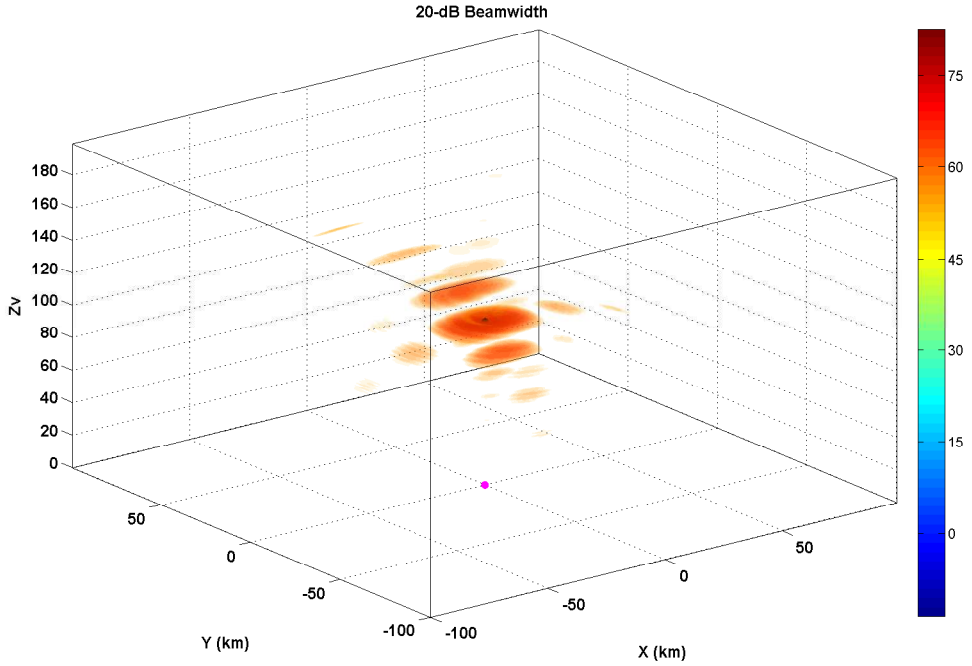

Figure 4.14: Composite receive pattern snapshot for a 9×9 FDA for 20-dB beamwidth.

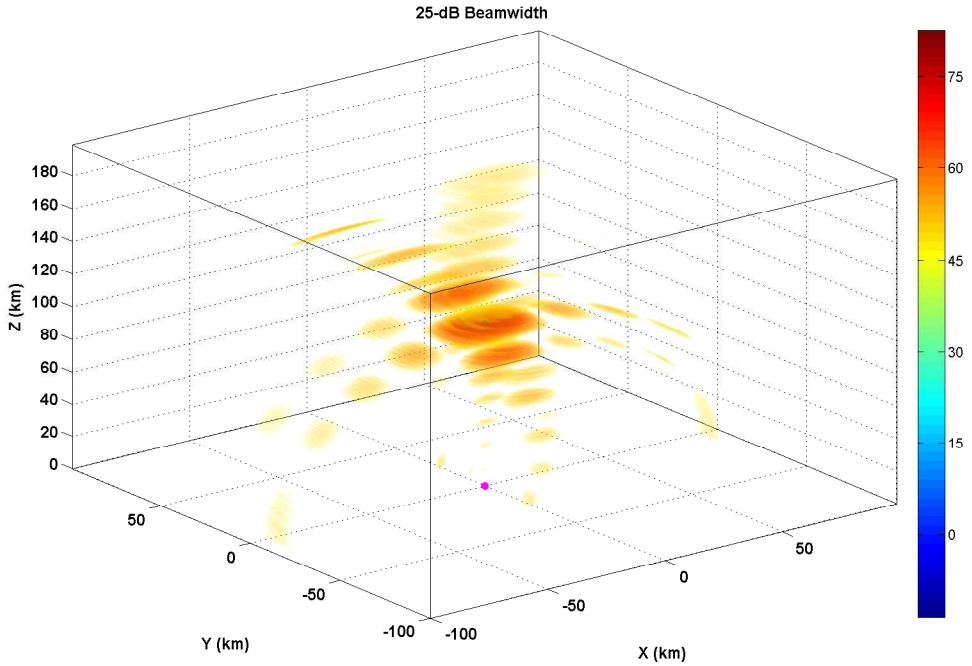

Figure 4.15: Composite receive pattern snapshot for a 9×9 FDA for 25-dB beamwidth.

Chapter 5

Multiple Beam Transmit and Receive with Coding

Progressively, fielded systems will need to perform multiple operations simultaneously and as system expectations are increased, the need for more complex signaling schemes will arise. Here, we propose the use of multi-beam FDA radar with waveform coding as an example of tackling this issue. Multi-beam radar is a familiar concept and has been previously used to accomplish simultaneous tracking and search or acquisition functions [**?**]. However, it has not been explored when additional complexities in the spatial patterns arise, such as cross-beam interference, as is the case with FDA radars. To mitigate these complications, we suggest applying coding on each beam to accompany the frequency coding at each transmit element to enable separation at the receiver after a decoding effort occurs.

This chapter discusses a possible scenario and the simulation set-up in section 5.1. In section 5.2, we develop the uncoded transmit and receive signals and spatial patterns, and provide analysis of challenges with this configuration. Section 5.3 provides description and analysis of the multiple beam coding scheme.

5.1 Geometry and Scenario

A simple scenario used for simulation purposes includes two stationary, steering directions (denoted as targets) represented in a 2-D polar coordinate system. A stationary, uniform linear array, multi-beam transceiver is used to illuminate the scene and Table 5.1 lists parameters used to simulate the spatial patterns. Figure 5.1 depicts this scenario and geometric set-up. We again assume the radar

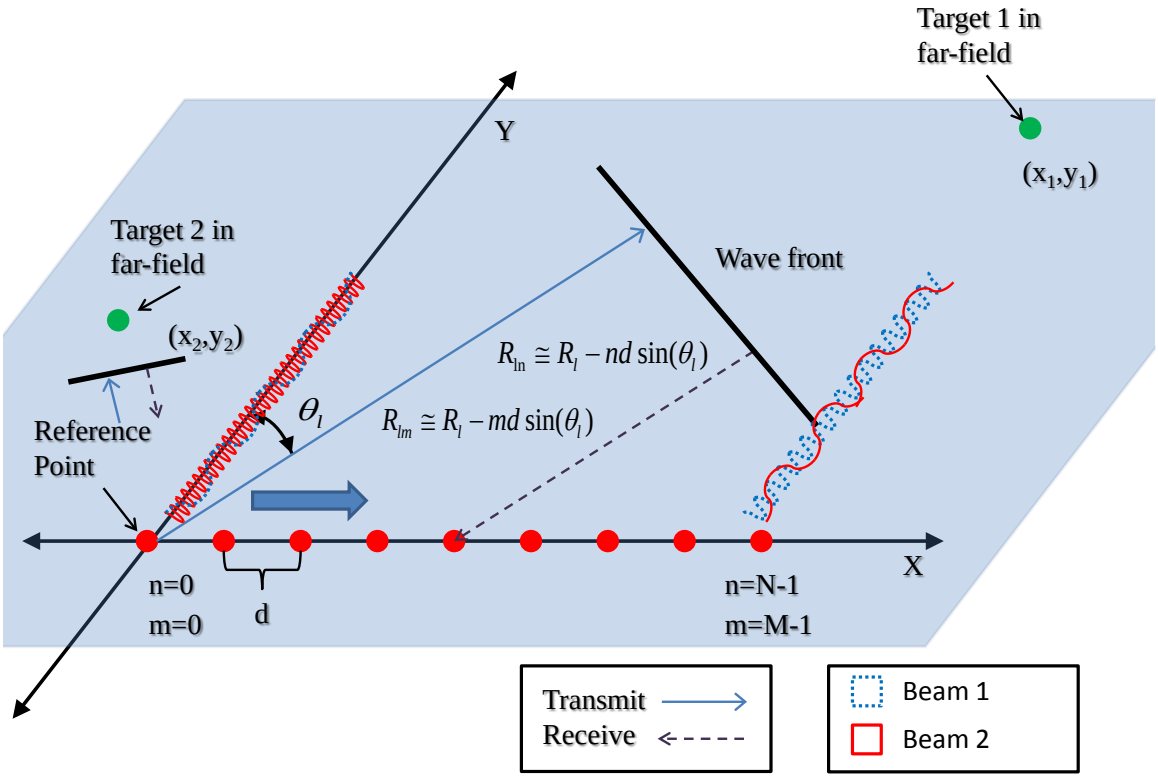

Figure 5.1: Scenario and set-up for two targets with independent beams steered to each location. The far-field approximation is made to estimate the phase of transmitted and received signals.

is operating in continuous wave (CW) mode and that graphics of the patterns are snapshots for fixed time t where $t \gg \frac{2R}{c}$, $2R$ is the two-way range of the furthest measured point, and c is the speed of light. The elements of the array are ideal isotropic radiators and without noise interference.

For this analysis, let the array span the X-axis with inter-element spacing $d = \frac{\lambda_{min}}{2}$, and set the Y-axis as the downrange axis such that the center of the array is located at $(d\frac{N-1}{2}, 0)$, where d is

Table 5.1: Parameters for multiple-beam simulations

Parameter	**Beam 1**	**Beam 2**
number TX elements N	9	9
number RX elements M	N	N
element spacing d	$\lambda_{min}/2 \cong 0.015$m	$\lambda_{min}/2 \cong 0.015$m
carrier frequency F_l	10 GHz	10 GHz
frequency offset Δf_l	2 kHz	-3 kHz
range grid limits	$[0, 200]$ km	$[0, 200]$ km
range grid spacing	2 km	2 km
azimuth grid limits	$[-90, 90]$ deg	$[-90, 90]$ deg
azimuth grid spacing	1 deg	1 deg
target range R_l	100 km	40 km
target azimuth θ_l	20 deg	-60 deg

the inter-element spacing ($d = \frac{\lambda_{min}}{2}$) again, see Figure 5.1. The FDA will transmit a set of linearly increasing or decreasing frequencies with step size Δf_l such that the set is succinctly represented as $f_{ln} = F_l + n\Delta f_l$ for $n = 0...N-1$ and $l = 1...L$, where F_l is the carrier for each beam (in our case $F_1 = F_2$) , N is the number of elements in the array, and L is the number of simultaneous beams.

We note that the simulations do not take into account mutual or self coupling, noise effects, non-ideal radiators or complex targets. Additionally, we assume perfect signal isolation where filters are involved.

5.2 Uncoded Transmit and Receive Signals

We present the transmit and receive patterns first, without the coding scheme, to provide context to the necessity of the coding technique. It is important to note that for the transmit and receive patterns, the beam forming is assumed to be done digitally, and that we are superimposing two pattern structures rather than optimizing the degrees of freedom available to achieve some metric.

5.2.1 Transmit Signal Structure

The signal transmitted for the l^{th} beam by the n^{th} emitter is a simple sinusoid given as

$$s_{ln}(t) = \exp\{j2\pi f_{ln} t\}, \tag{5.1}$$

and when delayed to a target location is

$$s_{ln}(t) = \exp\left\{j2\pi f_{ln}\left(t - \frac{R_n}{c}\right)\right\}, \tag{5.2}$$

The signal is measured for targets at coordinate sets (x_l, y_l) and element locations $(x_n, 0)$ by setting the range for each target l from each transmit element n as $R_n = \sqrt{(x - x_n)^2 + y^2}$. Letting the reference point be $(0, 0)$ and making a far-field approximation, we express range as $R_{ln} \cong R_l - nd\sin\theta_l$ where $R_l = \sqrt{x_l^2 + y_l^2}$, $\tan\theta_l = \frac{x_l}{y_l}$ and boresight is measured perpendicular to the reference element along the Y-axis, refer back to Fig 5.1.

In order to beamform on transmit, an additional phase term is necessary that comprises two components (angle and range). We steer the beam in angle $\hat{\theta}_l$ and range $\hat{R}_l$ to yield a composite beam-weighting factor $\alpha_{ln}(\hat{R}_l, \hat{\theta}_l) = \exp\{j2\pi f_{ln}(\frac{\hat{R}_l}{c} - \frac{nd\sin\hat{\theta}_l}{c})\}$, where $\hat{\theta}_l$ and $\hat{R}_l$ are relative to the reference element. The transmit signal from a single element as seen by a point target in space is

$$\begin{aligned} s_{ln}(t; \hat{R}_l, \hat{\theta}_l) &= \alpha_{ln}(\hat{R}_l, \hat{\theta}_l) s_{ln}\left(t - \frac{R_{ln}}{c}\right), \\ &= \exp\left\{j2\pi f_{ln}\left(\frac{\hat{R}_l}{c} - \frac{nd\sin\hat{\theta}_l}{c}\right)\right\} \times \\ &\exp\left\{j2\pi f_{ln}\left(t - \frac{R_l}{c} + \frac{nd\sin\theta_l}{c}\right)\right\}, \\ &= \exp\left\{j2\pi f_{ln}\left(t - \frac{R_l - \hat{R}_l}{c} + \frac{nd(\sin\theta_l - \sin\hat{\theta}_l)}{c}\right)\right\}. \end{aligned} \tag{5.3}$$

Using this, we create the total composite signal at a point in space by summing over all elements, and beams, in the ULA, making a far-field approximation and assuming narrowband operation this

is given as

$$
\begin{aligned}
s(t;\hat{R}_l,\hat{\theta}_l) &= \sum_{l=1}^{L}\sum_{n=0}^{N-1}\exp\left\{j2\pi f_{ln}\left(t-\frac{R_l-\hat{R}_l}{c}+\frac{nd(\sin\theta_l-\sin\hat{\theta}_l)}{c}\right)\right\}, \\
&\cong \exp\left\{j\Phi_l\right\}\times\sum_{l=1}^{L}\exp\left\{j2\pi\frac{R_l-\hat{R}_l}{\lambda_c}\right\}\times \\
&\frac{\sin\left(\omega_f N\left(t-\frac{R_l-\hat{R}_l}{c}\right)+\omega_o N(\sin\theta_l-\sin\hat{\theta}_l)\right)}{\sin\left(\omega_f\left(t-\frac{R_l-\hat{R}_l}{c}\right)+\omega_o(\sin\theta_l-\sin\hat{\theta}_l)\right)},
\end{aligned}
\tag{5.4}
$$

where $\omega_f = \pi\Delta f$, $\omega_l = \frac{\pi d}{\lambda_l}$. The term $\exp\{j\Phi_l\}$ contains additional phase factors associated with the geometry of the set-up.

In Figure 5.2, the spatial pattern for a CF ($\Delta f = 0$) and FDA with two beams steered to the target locations is shown. Notice, the CF pattern has no range dependency, only azimuth, while the FDA is periodic in both range and azimuth and has cross-beam interference.

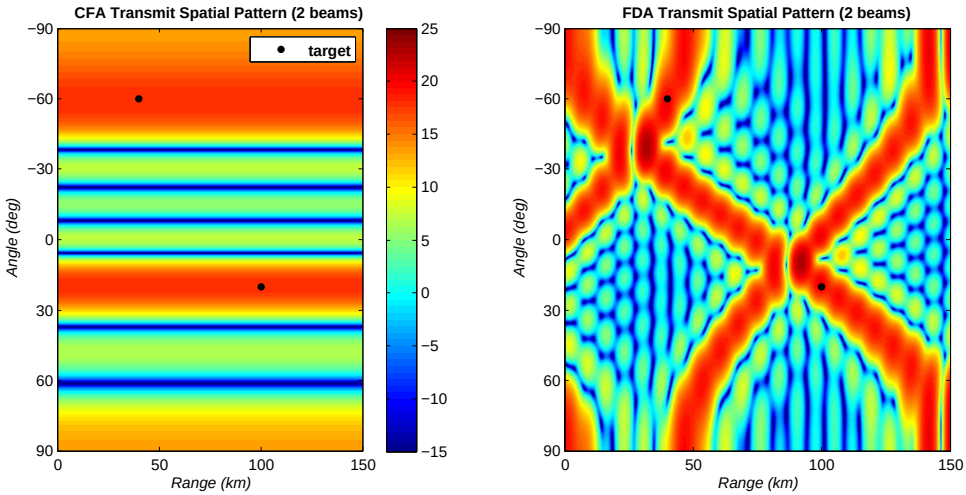

Figure 5.2: (left) CF spatial pattern for two beams with no range dependency, only azimuth. (right) FD spatial pattern for two beams with cross-beam interference and range and azimuth dependency.

5.2.2 Receive Signal Structure

The receive signal structure, without coding, for a completely frequency orthogonal array, requires a set of filter banks, each denoted H_m, at each element in order to apply the correct beam steering

phase shift for each beam, see Fig 5.3 for a representative block diagram.

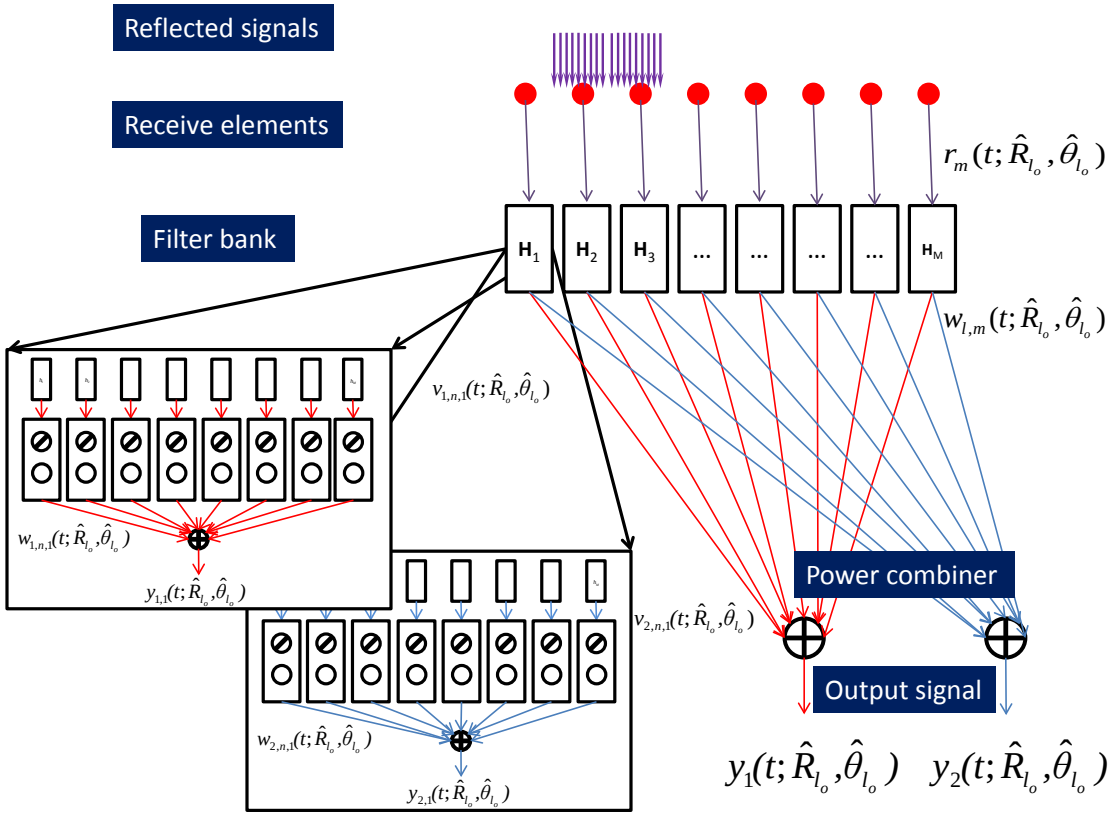

Figure 5.3: Beamforming chain with filter structures for two beams. Components include: filter banks at each element for each beam with a beamsteering mechanism and power combiners.

To begin, the transmit signal $s_{ln}(t;\hat{R}_l,\hat{\theta}_l)$ is unchanged, and the subsequent, unprocessed, received signal that enters filter bank H_m seen at element m is,

$$\begin{aligned} r_m(t;\hat{R}_l,\hat{\theta}_l) &= \sum_{l=1}^{L}\sum_{n=0}^{N-1} s_{ln}\left(t-\frac{2R_l}{c};\hat{R}_l,\hat{\theta}_l\right), \\ &\cong \sum_{l=1}^{L}\sum_{n=0}^{N-1} \exp\left\{j2\pi f_{ln}\left(t-\frac{2R_l-\hat{R}_l}{c}+\right.\right. \\ &\left.\left.\frac{nd(\sin\theta_l-\sin\hat{\theta}_l)}{c}+\frac{md\sin\theta_l}{c}\right)\right\}. \end{aligned} \tag{5.5}$$

The signal for the l^{th} beam from the n^{th} transmitter is output from filter h_{ln} (assuming no cross-talk

at the element level or frequency repetition) at the m^{th} receive element, and is given as

$$\begin{aligned} v_{lnm}(t;\hat{R}_l,\hat{\theta}_l) &= h_{ln}\{r_m(t;\hat{R}_l,\hat{\theta}_l)\}, \\ &= \exp\left\{j2\pi f_{ln}\left(t-\frac{2R_l}{c}+\frac{\hat{R}_l}{c}+\right.\right. \\ &\left.\left.\frac{nd(\sin\theta_l-\sin\hat{\theta}_l)}{c}+\frac{md\sin\theta_l}{c}\right)\right\}. \end{aligned} \tag{5.6}$$

Continuing, the filtered and beam-weighted signal for the l^{th} beam, out of the n^{th} beamformer at the m^{th} receive element is given as

$$\begin{aligned} w_{lnm}(t;\hat{R}_l,\hat{\theta}_l) &= \beta_{lnm}(\hat{R}_l,\hat{\theta}_l)v_{lnm}(t;\hat{R}_l,\hat{\theta}_l), \\ &= \exp\left\{j2\pi f_{ln}\left(t-\frac{2(R_l-\hat{R}_l)}{c}+\right.\right. \\ &\left.\left.\frac{nd(\sin\theta_l-\sin\hat{\theta}_l)}{c}+\frac{md(\sin\theta_l-\sin\hat{\theta}_l)}{c}\right)\right\}, \end{aligned} \tag{5.7}$$

where $\beta_{lnm}(\hat{R}_l,\hat{\theta}_l)=\exp\{j2\pi f_{ln}(\frac{\hat{R}_l}{c}-\frac{md\sin\hat{\theta}_l}{c})\}$. The last component of the filter bank stage is the combiner, where the output is given as

$$\begin{aligned} y_{lm}(t;\hat{R}_o,\hat{\theta}_o) &= \sum_{n=0}^{N-1} w_{lnm}(t;\hat{R}_l,\hat{\theta}_l), \\ &= \sum_{n=0}^{N-1}\exp\left\{j2\pi f_{ln}\left(t-\frac{2(R_l-\hat{R}_l)}{c}+\right.\right. \\ &\left.\left.\frac{nd(\sin\theta_l-\sin\hat{\theta}_l)}{c}+\frac{md(\sin\theta_l-\sin\hat{\theta}_l)}{c}\right)\right\}. \end{aligned} \tag{5.8}$$

At this point in the beamforming, we are exiting the filter bank stage and all that remains is to combine the signal from each beam for all filter banks. The composite signal is computed as a sum over N receivers of signals from N transmitters that have been delayed out and back ($\frac{2R_l}{c}$) from a target, steered on transmit ($\frac{\hat{R}_l-nd\sin\hat{\theta}_l}{c}$) and then steered on receive by matching the frequency f_{ln} with the appropriate steering associated with each receive element m and beam l to yield separate

signals

$$
\begin{aligned}
y_l(t;\hat{R}_o,\hat{\theta}_o) &= \sum_{m=0}^{N-1} y_{lm}(t,\hat{R}_l,\hat{\theta}_l), \\
&= \sum_{m=0}^{N-1}\sum_{n=0}^{N-1} \exp\left\{ j2\pi f_{ln}\left(t - \frac{2(R_l-\hat{R}_l)}{c} + \right.\right. \\
&\left.\left. \frac{nd(\sin\theta_l - \sin\hat{\theta}_l)}{c} + \frac{md(\sin\theta_l - \sin\hat{\theta}_l)}{c} \right) \right\}.
\end{aligned} \tag{5.9}
$$

This technique will yield unique spatial patterns for each beam, under the previously stated assumption of no cross-talk, that is separable frequency coding at the element level, (see Figure 5.4).

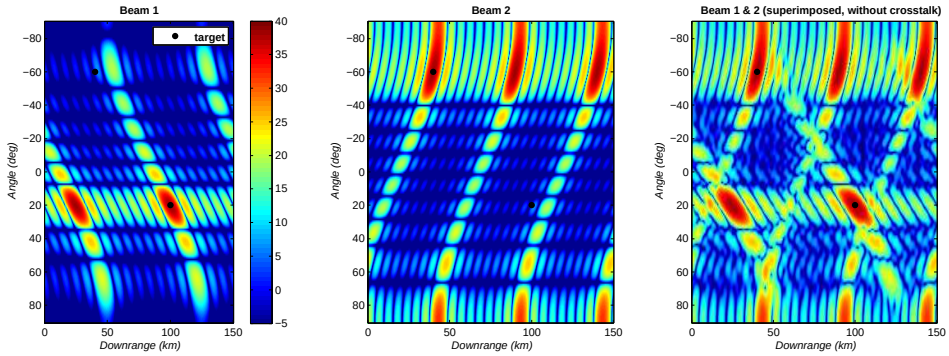

Figure 5.4: (left) Beam 1 spatial pattern without cross-talk. (middle) Beam 2 receive spatial pattern without cross-talk. (right) Composite receive spatial pattern without cross-talk.

However, without frequency separation, we observe cross-talk among the signals. The superimposed spatial pattern (right side of Figure 5.4) is given by equation (5.10). This equation is the summation of the two spatial patterns when each beam is considered separate. This spatial pattern shows multiple cross-beam interference peaks, the real catalyst for pursuing alternate beamforming schemes, and it is obvious that the range-angle dependent main beam coherence phenomenon would

disrupt the radar signal processing.

$$
\begin{aligned}
y(t;\hat{R}_o,\hat{\theta}_o) \cong \exp\left\{j\Psi\right\} \times \sum_{l=1}^{L} \exp\left\{j2\pi \frac{2(R_l-\hat{R}_l)}{\lambda_c}\right\} \times \\
\frac{\sin\left(\omega_o N(\sin\theta_o - \sin\hat{\theta}_o)\right)}{\sin\left(\omega_o(\sin\theta_o - \sin\hat{\theta}_o)\right)} \times \\
\frac{\sin\left(\omega_f N(t - 2\frac{R_o-\hat{R}_o}{c}) + \omega_o N(\sin\theta_o - \sin\hat{\theta}_o)\right)}{\sin\left(\omega_f(t - 2\frac{R_o-\hat{R}_o}{c}) + \omega_o(\sin\theta_o - \sin\hat{\theta}_o)\right)}.
\end{aligned}
\tag{5.10}
$$

With slight frequency overlap, an example is given for the parameters in Table 5.1, where the only overlap is at the carrier $F_1 = F_2$. As shown in Fig 5.5, separate beams compared to the single beam operation, a range-angle smearing effect is perceived as the carrier signal component from each beam is seen by both beams. This issue could only be exacerbated by real-world issues such as Doppler, spectral leakage, correlated noise and other undesirable repeated frequencies.

We also assume infinitely narrow bandwidth when developing the signal model which does not address the Doppler shift associated with potentially in-bound and out-bound targets simultaneously, but on different beams. In order to protect the integrity of the return signals information, we propose on additional layer of orthogonality by applying a code sequence at the beam level.

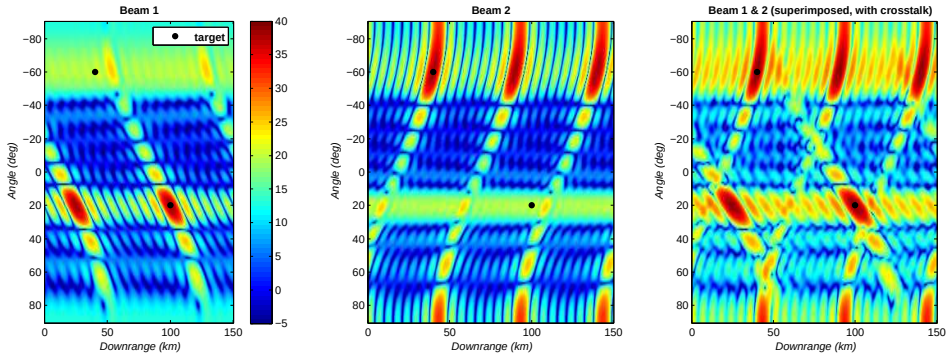

Figure 5.5: (left) Beam 1 spatial pattern with cross-talk at F_1. (middle) Beam 2 receive spatial pattern with cross-talk at F_2. (right) Composite receive spatial pattern with cross-talk.

5.3 Coding Technique

In this section, we outline applying a circularly orthogonal code sequence at the beam level to enable separation of multiple beams. The receive processing chain is shown in Figure 5.6 with a decoder and complete filter bank for each beam frequency.

The signal transmitted for the l^{th} beam by the n^{th} emitter is a sinusoidally-modelled code sequence given as

$$s_{ln}(t) = c_l(t) \exp\{j2\pi f_{ln} t\}, \tag{5.11}$$

and when delayed to a steered location is

$$s_{ln}(t) = c_l\left(t - \frac{R_n}{c}\right) \exp\left\{j2\pi f_{ln}\left(t - \frac{R_n}{c}\right)\right\}, \tag{5.12}$$

where signal $c_l(t)$ contains circularly orthogonal sequences. For simulation purposes, we use codes of length 128 that are sampled at $f_s = 10$ MHz.

Using the same development procedure as in the linear array and planar array signal model development, the composite multiple beam signal propagated to the target location is given as

$$\begin{aligned} s(t; \hat{R}_l, \hat{\theta}_l) = \sum_{l=1}^{L} \sum_{n=0}^{N-1} c_l\left(t - \frac{R_l}{c} + \frac{nd\sin\theta_l}{c}\right) \times \\ \exp\left\{j2\pi\Big(F_l + n\Delta f_l\Big)\left(t - \frac{R_l - \hat{R}_l}{c} + \frac{nd(\sin\theta_l - \sin\hat{\theta}_l)}{c}\right)\right\}. \end{aligned} \tag{5.13}$$

Then, the receive signal model, at each element, prior to the decoding and filter process is given as

$$\begin{aligned} r_m(t; \hat{R}_l, \hat{\theta}_l) = \sum_{l=1}^{L} \sum_{n=0}^{N-1} c_l\left(t - \frac{2R_l}{c} + \frac{nd\sin\theta_l}{c} + \frac{md\sin\theta_l}{c}\right) \times \\ \exp\left\{j2\pi\Big(F_l + n\Delta f_l\Big)\left(t - \frac{2R_l}{c} + \frac{\hat{R}_l}{c} + \right.\right. \\ \left.\left.\frac{nd(\sin\theta_l - \sin\hat{\theta}_l)}{c} + \frac{md\sin\theta_l}{c}\right)\right\}. \end{aligned} \tag{5.14}$$

This signal enters a matched filter bank and combines outputs from all receiver elements to give two distinct beams, one for each code sequence. Equation 5.15 gives the signal model for each

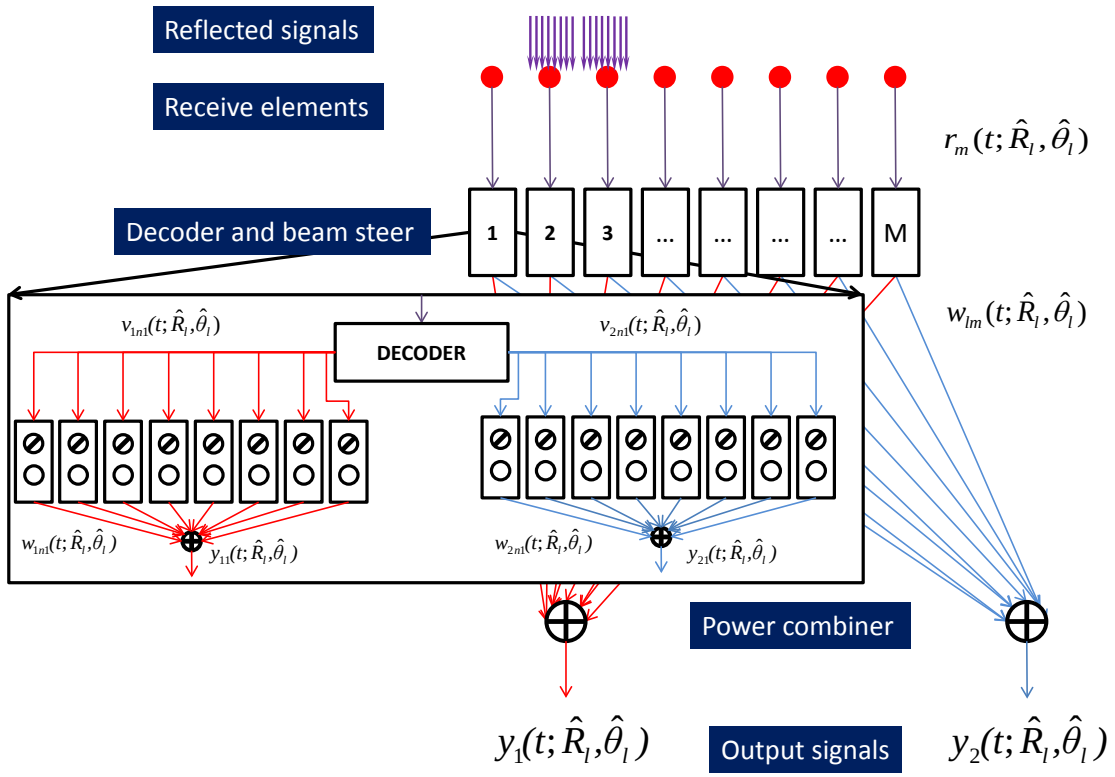

Figure 5.6: Receive processing chain for the amplitude and frequency coding multiple beam scheme.

beam as

$$
\begin{aligned}
y_l(t;\hat{R}_l,\hat{\theta}_l) = \sum_{t=1}^{T}\sum_{m=0}^{M-1}\sum_{n=0}^{N-1} c_l^*\left(t - \frac{2\hat{R}_l}{c} + \frac{nd\sin\hat{\theta}_l}{c} + \frac{md\sin\hat{\theta}_l}{c}\right)\times \\
c_l\left(t - \frac{2R_l}{c} + \frac{nd\sin\theta_l}{c} + \frac{md\sin\theta_l}{c}\right)\times \\
\exp\left\{j2\pi\Big(F_l + n\Delta f_l\Big)\left(t - \frac{2(R_l-\hat{R}_l)}{c}\times\right.\right. \\
\left.\left. + \frac{nd(\sin\theta_l - \sin\hat{\theta}_l)}{c} + \frac{md(\sin\theta_l - \sin\hat{\theta}_l)}{c}\right)\right\} \\
\cong C\exp\Big\{j\Psi\Big\}\times\frac{\sin\Big(\omega_o N(\sin\theta_o - \sin\hat{\theta}_o)\Big)}{\sin\Big(\omega_o(\sin\theta_o - \sin\hat{\theta}_o)\Big)}\times \\
\frac{\sin\Big(\omega_f N(t - 2\frac{R_o-\hat{R}_o}{c}) + \omega_o N(\sin\theta_o - \sin\hat{\theta}_o)\Big)}{\sin\Big(\omega_f(t - 2\frac{R_o-\hat{R}_o}{c}) + \omega_o(\sin\theta_o - \sin\hat{\theta}_o)\Big)}.
\end{aligned}
\tag{5.15}
$$

Where $c_l^*(t)$ is the conjugate code sequence delayed on receive by the estimated range and T is the discrete number of time samples over which the code sequence is matched and C is the integration amplitude scaling factor. By observing the pattern response over an extended amount of time, we incur unaccounted for self-interference phase mismatches at the receiver due to the time dependency of the FDA pattern. However, for the relatively small offset in our simulations this would not be an issue, therefore the negligible time dependent smearing effect is not modeled.

Figure 5.7 shows the transmit beam patterns for each beam separately and the total spatial response for the coded signal model. Figure 5.8 shows the composite transmit and receive spatial response for both beams out of the matched filter.

It is clear that the additional layer of orthogonality further enables separation at the beam level, mitigating the cross beam interference sidelobes substantially. In the case where each beam operates on the same carrier and offset ($F_1 = F_2$, $\Delta f_1 = \Delta f_2$), Figure 5.9 shows the matched filter responses and clearly, the two beams are separable.

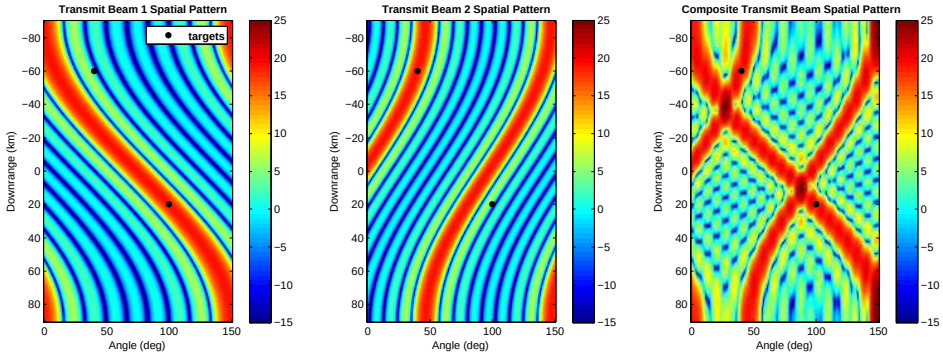

Figure 5.7: (left) Beam 1 coded transmit spatial pattern. (middle) Beam 2 coded transmit spatial pattern. (right) Composite coded transmit pattern.

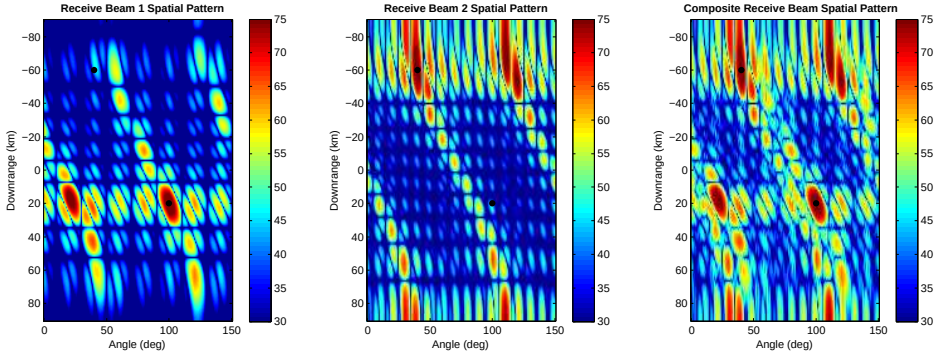

Figure 5.8: (left) Beam 1 coded transmit spatial pattern. (middle) Beam 2 coded transmit spatial pattern. (right) Composite coded transmit pattern.

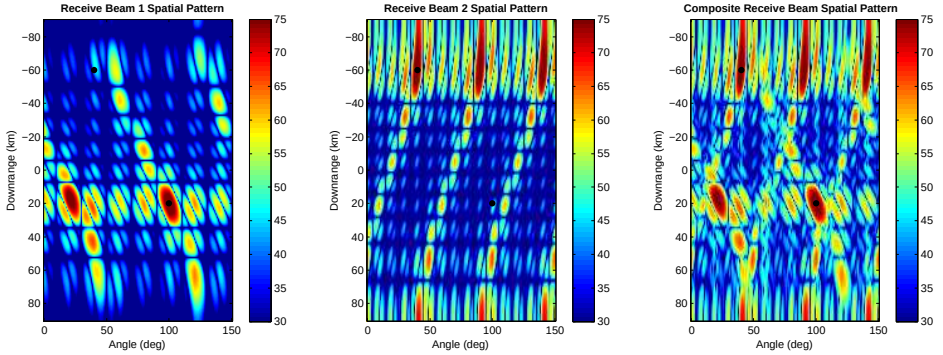

Figure 5.9: (left) Beam 1 coded transmit spatial pattern ($\Delta f_1 = \Delta f_2$). (middle) Beam 2 coded transmit spatial pattern ($\Delta f_1 = \Delta f_2$). (right) Composite coded transmit pattern ($\Delta f_1 = \Delta f_2$).

Chapter 6

Conclusions and Future Work

In this thesis, we discussed the need for multi-mission, multi-mode capable radar systems and the inherent ability of the FDA to satiate this requirement.

In Chapter 3, we developed the signal structures for three architectures for transmitting and receiving on a FDA system and analyzed each for their design complexity and spatial pattern structures. The band-limited, coherent FDA technique would generally not be practical for systems with power limitation concerns. Although, because this architecture requires the simplest hardware configuration and does steer the beam to the target location, it may have some potential applications. The full-band, pseudo-coherent FDA technique also has a simple hardware configuration, but does not steer the receive beam to the target location and therefore would not be a practical system. Additional analysis of steering the beam strictly by modulating the offset frequency Δf is warranted, as this would simplify the required hardware needed to implement this type of system. The full-band, coherent FDA contains all spatial and frequency information on each receive channel from each transmit element and beamforms to place maximum signal at the target location. This is the most complex architecture, but provides a mechanism to steer the beam in range and azimuth that contains all received energy.

In Chapter 4, we extended the concept of the linear array to planar geometries and suggested a notional transmit set-up where only a single Δf was required but scaled for each transmit element such that each frequency was unique. Using a filter bank approach on receive we generated receive spatial patterns that isolated the main beam responses in angle and range, a first in multi-dimensional

beamforming. These patterns are extremely unique and are even more complex than what is visualized due to additional sidelobe structure greater than 10-dB off the peak. Also, with this additional degree of freedom it has been suggested that 3-D null steering, or null steering in range could be possible [27]. Additionally, it could warrant multiple target tracking at different azimuths, elevations and ranges within a single beam, although this may require a different receiver architecture. While these ideas seem probable, there is also the issue of periodicity and time dependence for this type of pattern. It is currently being investigated if the time dependency could be eliminated while still maintaining the range-angle dependency. Moving forward, we also suggest investigation of more complex waveform schemes, such as exponential or other non-linear frequency offsets in an effort to improve main beam peak-to-sidelobe ratio.

Finally, we presented a transceiver technique to enable separation of multiple range-dependent beams in Chapter 5 that applied an additional level of orthogonality with an amplitude coding sequence. While diversity domain exploitation is a familiar concept, we aimed to show it could be applied to range-dependent spatial patterns successfully. We have outlined a potential technique and architecture to perform multiple beam FDA radar and separate the spatial responses on receive for a CW system. We have shown the patterns that arise from simulation for both the coded and uncoded to provide context for additional signal orthogonality. This concept could also easily be scaled to incorporate a number beams and into a planar geometry, assuming the aforementioned concerns on self-interference over a code cycle are heeded.

The future of FDA will depend on the ability of the designer to control the time dependency of the spatial response. It is proposed that by applying phase shifts, in addition to steering the beam to the target location, the time dependency could be mitigated while maintaining the angle-range relationships. It is also proposed that the planar receive pattern, refer back to Figure 4.9, an orb-like pattern surrounding the target, could be generated on transmit, further reducing the unwanted responses away from the target.

Bibliography

[1] P. Antonik, M. Wicks, H. Griffiths, and C. Baker, "Frequency diverse array radars," in *Radar, 2006 IEEE Conference on*, p. 3 pp., 2006.

[2] P. Antonik, *An investigation of a frequency diverse array*. PhD thesis, University College London United Kingdom, May 2009.

[3] P. Antonik, M. Wicks, H. Griffiths, and C. Baker, "Multi-mission multi-mode waveform diversity," in *Radar, 2006 IEEE Conference on*, p. 3, IEEE, 2006.

[4] M. Wicks and P. Antonik, "Frequency diverse array with independent modulation of frequency, amplitude, and phase." http://www.freepatentsonline.com/7319427.html, January 2008.

[5] M. Wicks and P. Antonik, "Method and apparatus for a frequency diverse array." http://www.freepatentsonline.com/7511665.html, March 2009.

[6] M. Secmen, S. Demir, A. Hizal, and T. Eker, "Frequency diverse array antenna with periodic time modulated pattern in range and angle," in *Radar Conference, 2007 IEEE*, pp. 427–430, IEEE, 2007.

[7] J. Huang, K. Tong, and C. Baker, "Frequency diverse array with beam scanning feature," in *Antennas and Propagation Society International Symposium, 2008. AP-S 2008. IEEE*, pp. 1–4, IEEE, 2008.

[8] Jingjing Huang and Kin-Fai Tong and Baker, C., "Frequency diverse array: Simulation and design," in *Antennas Propagation Conference, 2009. LAPC 2009. Loughborough*, pp. 253 – 256, Nov. 2009.

[9] S. Brady and A. F. I. O. T. W.-P. A. O. S. O. ENGINEERING, "Frequency Diverse Array Radar: Signal Characterization and Measurement Accuracy," 2010.

[10] J. Farooq, M. Temple, and M. Saville, "Application of frequency diverse arrays to synthetic aperture radar imaging," in *Electromagnetics in Advanced Applications, 2007. ICEAA 2007. International Conference on*, pp. 447–449, IEEE, 2007.

[11] P. Baizert, "Forward-looking Radar Clutter Suppression using Frequency Diverse Arrays," Master's thesis, Air Force Institue of Technology, March 2006.

[12] J. Farooq, M. Temple, and M. Saville, "Exploiting frequency diverse array processing to improve SAR image resolution," in *Radar Conference, 2008. RADAR'08. IEEE*, pp. 1–5, IEEE, 2008.

[13] J. Farooq, "Frequency Diversity for Improving Synthetic Aperture Radar Imaging," tech. rep., AIR FORCE INST OF TECH WRIGHT-PATTERSON AFB OH GRADUATE SCHOOL OF ENGINEERING AND MANAGEMENT, 2009.

[14] P. Sammartino and C. Baker, "The frequency diverse bistatic system," in *Waveform Diversity and Design Conference, 2009 International*, pp. 155–159, IEEE, 2009.

[15] P. Sammartino and C. Baker, "Developments in the Frequency Diverse Bistatic System," in *Radar Conference, 2009 IEEE*, pp. 1–5, IEEE, 2009.

[16] P. Sammartino, "A comparison of processing approaches for distributed radar sensing," *Open Access publications from University College London*, 2009.

[17] P. Sammartino, C. Baker, and H. Griffiths, "Range-angle dependent waveform," in *Radar Conference, 2010 IEEE*, pp. 511–515, IEEE, 2010.

[18] Browning, J.P. and Fuhrmann, D.R. and Rangaswamy, M., "A Hybrid Mimo Phased-Array Concept for Arbitrary Spatial Beampattern Synthesis," in *Digital Signal Processing Workshop and 5th IEEE Signal Processing Education Workshop, 2009. DSP/SPE 2009. IEEE 13th*, pp. 446 –450, Jan. 2009.

[19] Fuhrmann, D.R. and Browning, J.P. and Rangaswamy, M., "Adapting a MIMO/phased-array radar transmit beampattern to target location," in *Cognitive Information Processing (CIP), 2010 2nd International Workshop on*, pp. 354 –359, june 2010.

[20] Higgins, T. and Blunt, S.D., "Analysis of range-angle coupled beamforming with frequency-diverse chirps," in *Waveform Diversity and Design Conference, 2009 International*, pp. 140 –144, Feb. 2009.

[21] P. Baizert, T. Hale, M. Temple, and M. Wicks, "Forward-looking radar GMTI benefits using a linear frequency diverse array," *Electronics Letters*, vol. 42, no. 22, pp. 1311–1312, 2006.

[22] Chen Yong-guang and Li Yun-tao and Wu Yan-hong and Chen Hong, "Research on the linear frequency diverse array performance," in *Signal Processing (ICSP), 2010 IEEE 10th International Conference on*, pp. 2324 –2327, Oct. 2010.

[23] Long Zhuang and Xingzhao Liu and Wenxian Yu, "Precisely beam steering for frequency diverse arrays based on frequency offset selection," in *Radar Conference - Surveillance for a Safer World, 2009. RADAR. International*, pp. 1 –4, Oct. 2009.

[24] A. Aytun, "Frequency Diverse Array Radar," Master's thesis, Naval Postgraduate School, September 2010.

[25] D. Glass, "Matlab 4-d visualization technique." Personal correspondence, 2009.

[26] A. Jones and B. Rigling, "Frequency diverse array radar receiver architecures," in *Waveform Diversity and Design Conference, 2011 International*, IEEE, 2012.

[27] M. Rangaswamy, "Frequency diverse array range nulling capabilities." Personal correspondence, 2011.